Numer. Math. (2005) 101: 273–308
DOI 10.1007/s00211-005-0620-7

Numerische Mathematik

Andrea Cangiani · Endre Süli

Enhanced RFB method

Received: 23 April 2004 / Revised: 17 December 2004 / Published online: 5 July 2005

Abstract The *residual-free bubble method* (RFB) is a parameter-free stable finite element method that has been successfully applied to a wide range of boundary-value problems exhibiting multiple-scale behaviour. If some local features of the solution are known *a priori*, the approximation properties of the RFB finite element space can be improved by enriching it on selected edges of the partition by *edge-bubbles* that are supported on pairs of neighbouring elements. Motivated by this idea, we define and analyse an *enhanced residual-free bubble* method for the solution of convection-dominated convection-diffusion problems in 2-D. Our *a priori* analysis highlights the limitations of the RFB method and the improved global approximation properties of the new method. The theoretical results are supported by detailed numerical experiments.

1 Introduction

The underlying principle behind the use of *bubble methods* (see, e.g. [9]) is that of enriching the Galerkin finite element space with functions (bubbles) having compact support on every element of the given partition. The bubbles are successively eliminated through static condensation, leaving a generalised Galerkin scheme for the original finite element space which is expected to have improved approximation properties. In general, we expect this to be the case when the numerical solution of the problem under consideration is sensitive to features present on scales that cannot be represented on the given mesh. For instance, in the framework of boundary-value problems for convection-dominated convection-diffusion equations, bubble methods have proved successful in capturing subgrid-scale features,

A. Cangiani · E. Süli (✉)
Oxford University Computing Laboratory, Wolfson Building, Parks Road,
Oxford OX1 3QD, UK
E-mail: endre.suli@comlab.ox.ac.uk

such as thin internal and boundary layers, while recovering many classical stabilised finite element methods [7].

The *residual-free bubble method* [15, 8] is based on choosing as rich a bubble-space as possible. The resulting scheme has the desirable property of being locally residual free, i.e. it has a solution satisfying the differential equation under consideration inside every element.

A limitation of classical bubble methods in general, and of RFB in particular, is that only those subgrid features can be accurately modelled that do not cross the inter-element boundaries. As pointed out in [6], in circumstances when it is crucial that subgrid scales are accurately captured, bubble methods should benefit from the addition of *edge-bubbles*, i.e. bubbles with support on pairs of elements sharing an edge, the underlying criterion being that the number of such edge-bubbles is kept small relative to the total number of degrees of freedom (so as to ensure that the resulting computational overhead is negligible).

In the present paper we formalize this idea: by building on the *augmented-space* formulation of Brezzi & Marini [14], we define a new algorithm, the *enhanced residual-free bubble method* (RFBe), and develop its *a priori* error analysis. The proposed method is then successfully applied to convection-dominated diffusion problems. Here, we confine ourselves to problems where the subdomains within which edge-bubbles need to be used are known *a priori*. We refer to our recent work [16] for the construction of an *hb*-adaptive algorithm which performs adaptive mesh refinement in conjunction with an adaptive choice of the active bubbles, based on *a posteriori* error analysis.

The idea behind the present method is to combine the generality of a stabilised method with the specialized use of *ad hoc* finite elements constructed in a way to capture subgrid-scale behaviour on edges in the partition (see [24] and the references therein). A similar approach is developed in [3] and [4] for the discretisation of the convection term in the Navier–Stokes equations. The finite elements introduced in [3] are tensor products of one-dimensional exponential edge-functions which reflect the local flow conditions, so as to obtain a method that is accurate in all flow regimes. As recognized in [4], the edge-functions should be interpreted as one-dimensional bubbles (cf. [12]), and are, in turn, related to the *link-cutting bubbles* proposed in [11] for convection-diffusion-reaction problems in one space-dimension. A closely related technique is the Petrov–Galerkin method presented in [19] for the solution of reaction-diffusion problems, where, just as in the present method, residual-free bubbles are supplemented by suitable edge-functions with the aim to enhance the trial space.

This paper is devoted to the design and error analysis of the RFBe finite element method for convection-dominated diffusion problems. Briefly, the method is defined as follows. The RFB finite element space is enriched with edge-bubbles in subregions where layers are present. Specifically, on each element-edge, internal to the computational domain, that intersects an exponential boundary layer, the associated edge-bubble is defined as an exponential edge-function obtained by solving the projection of the original PDE onto the edge subject to homogeneous Dirichlet boundary conditions at the endpoints of the edge; on each of the two elements that share the edge, the edge-bubble is defined as the solution of the homogeneous partial differential equation obtained by restricting the original equation to the interior of the two elements, subject to suitable boundary conditions (i.e. homogeneous

Dirichlet boundary condition on all the edges of each of the two elements, except the shared edge where a non-homogeneous Dirichlet boundary condition is used, with the exponential edge-function as boundary datum).

We show through *a priori* analysis, and illustrate by numerical experiments, that the RFBe method improves the RFB resolution of boundary layers. A crucial property of the RFBe method is that the locally introduced edge-bubbles provide global improvement of the solution, indicating that the presence of edge-bubbles has a global stabilising effect. In addition, unlike standard stabilised finite element methods, the RFBe method accurately captures the behaviour of the solution inside boundary layers even on relatively coarse computational meshes. Our current implementation of the RFBe method does not supplement the basic RFB approximation with edge-bubbles within internal layers; its accuracy within internal layers is therefore no better than that of RFB (see Section 5). The inclusion of suitable edge-bubbles within internal layers would, of course, lead to further improvements in accuracy.

The paper is structured as follows. We present the method in Section 2, applying the general framework for multilevel methods proposed by Brezzi & Marini in [14]. In Section 3, we explain how the edge-bubbles are defined for convection-dominated convection-diffusion problems. Our choice is justified in Section 4 through *a priori* analysis. Finally, Section 5 is dedicated to the fully discrete version of the method (i.e. including the numerical approximation of the bubbles). The theoretical results are confirmed by numerical experiments.

2 A framework for the enrichment of the RFB finite element method

Given a bounded polygonal domain Ω in $\mathbb{R}^2$, let $\mathcal{L}(\cdot,\cdot)$ be a bounded coercive bilinear functional on $V = \mathrm{H}_0^1(\Omega)$ and let $f \in \mathrm{L}^2(\Omega)$. We consider the elliptic boundary-value problem in variational form:

$$\begin{cases} \text{find } u \in V \text{ such that} \\ \mathcal{L}(u, v) = (f, v) \qquad \forall v \in V. \end{cases} \tag{1}$$

Assume that we are given a family $\{\mathcal{T}_h\}$ of conforming and shape-regular partitions $\mathcal{T}_h$ of $\overline{\Omega}$ such that any $T \in \mathcal{T}_h$ is affine-equivalent to a reference element $\widehat{T}$ through an affine map F_T. Finally, let h be the discretisation parameter, i.e. the maximum elemental diameter.

We define, over $\mathcal{T}_h$, the standard finite element space V_h of all piecewise linear functions (if $\hat{T}$ is an open unit triangle) or piecewise bilinear functions (if $\hat{T}$ is an open unit square). Moreover, let B_h be the space of residual-free bubbles, i.e. the set of all functions in V that vanish on the skeleton of the partition $\mathcal{T}_h$. That is, we define

$$\begin{aligned} V_h &= \big\{ v_h \in \mathrm{H}_0^1(\Omega) : w_{h|_T} \in \mathcal{P}_1(T) \\ &\qquad\qquad (\text{or } w_{h|_T} \circ F_T \in \mathcal{Q}_1(\hat{T})) \quad \forall T \in \mathcal{T}_h \big\}, \\ B_h &= \bigoplus_{T \in \mathcal{T}_h} \mathrm{H}_0^1(T). \end{aligned} \tag{2}$$

The *residual-free bubble* finite element space is then defined as $V_{\text{RFB}} = V_h \oplus B_h$, the direct sum being ensured since V_h does not contain nontrivial bubbles, i.e. $V_h \cap B_h = \{0\}$.

We mention here that it is possible to define higher-order residual-free bubble finite element spaces, the general recipe being that the bubble-space should be as large as possible, as explained by Brezzi in [6].

The residual-free bubble method (RFB) is given by restricting (1) to the subspace V_{RFB}:

$$\begin{cases} \text{find } u_{\text{RFB}} \in V_{\text{RFB}} \text{ such that} \\ \mathcal{L}(u_{\text{RFB}}, v) = (f, v) \qquad \forall v \in V_{\text{RFB}}. \end{cases} \tag{3}$$

Thanks to the richness of the space of bubbles B_h, the solution u_{RFB} has the desirable property of being residual-free on the interior of any element (see [13]).

As we shall see later, the bubble part of the solution can be eliminated, at least formally, from the RFB formulation through a static condensation procedure which leads to a generalised Galerkin formulation over the standard finite element space V_h. In other words, the RFB method can be formulated as a two-level algorithm which corresponds to a sort of divide-and-conquer principle: the space of bubbles B_h should take into account the fine scales of the problem while the solution on V_h gives an approximation of the global behaviour of u.

The draw-back of such a two-level procedure is that only the small scales that do not cross the boundary of any element of the partition will be taken into account. Thus, following an idea by Brezzi [6], we propose to further enrich the RFB space with the aim of improving the approximation properties on the skeleton of the partition. The framework is that of the general augmented-space method proposed by Brezzi and Marini in [14], which is defined as follows.

Let Σ be the skeleton of our partition $\mathcal{T}_h$, i.e. the union of the boundaries of all elements in $\mathcal{T}_h$, and let Φ be the space of traces of V on Σ. An *augmented subspace* is defined by considering all the extensions onto $\overline{\Omega}$ from a finite-dimensional subspace of Φ. That is, given a subspace $\Phi_h \subset \Phi$ of finite dimension, we define the space

$$V_a := \left\{ v \in V \,:\, v_{|\Sigma} \in \Phi_h \right\}.$$

The *augmented-space formulation* is obtained by restricting (1) to V_a:

$$\begin{cases} \text{find } u_a \in V_a \text{ such that} \\ \mathcal{L}(u_a, v_a) = (f, v_a) \qquad \forall v_a \in V_a. \end{cases} \tag{4}$$

The existence and uniqueness of the solution to (4) are ensured by the continuity and coercivity of the bilinear functional $\mathcal{L}$ over $V_a \times V_a$, by virtue of the Lax–Milgram theorem.

By definition of V_{RFB}, the augmented space V_a always contains as a subspace the residual-free bubble-space B_h as defined in (2). Further, the RFB method is obtained from the above general formulation simply by choosing Φ_h as the space spanned by the traces of V_h.

We can also identify a second subspace V_l, which depends on the bilinear functional $\mathcal{L}$:

$$V_l := \{ v_l \in V_a \,:\, \mathcal{L}(v_l, v_b) = 0 \quad \forall v_b \in B_h \}, \tag{5}$$

and observe that we have the splitting

$$V_a = V_l \oplus B_h. \tag{6}$$

In the special case when V_a is equal to V_{RFB}, we also have, by definition,

$$V_a = V_{\text{RFB}} = V_h \oplus B_h.$$

Since V_h and V_l are not equal, the two characterisations of the RFB space are different. Thus, the augmented-space formulation naturally gives a new interpretation to the RFB method. Indeed, the solution u_a of (4) can be characterised as follows (see [14]).

Theorem 1 *Let u_a be the unique solution of (4). Then, its decomposition according to (6) is given by $u_a = u_l + u_b^f$ where u_b^f is the unique solution in B_h of*

$$\mathcal{L}(u_b^f, v_b) = (f, v_b) \qquad \forall v_b \in B_h, \tag{7}$$

and u_l is the unique solution in V_l of

$$\mathcal{L}(u_l, v_l) + \mathcal{L}(u_b^f, v_l) = (f, v_l) \qquad \forall v_l \in V_l. \tag{8}$$

Remark 1 The *bubble equation* (7), i.e. the equation obtained from the augmented-space formulation by testing in the bubble-space, has the appealing property of being independent of u_l. Moreover the two equations (7) and (8) decouple if $\mathcal{L}$ is a symmetric (bilinear) functional, since in this case $\mathcal{L}(u_b^f, v_l) = \mathcal{L}(v_l, u_b^f) = 0$ by (5).

2.1 General definition of the RFBe method

The formulation (4) represents a framework for the modification of the RFB method. We mentioned already that the RFB method is obtained from the augmented-space formulation by choosing $\Phi_h = V_h|_\Sigma$: we now modify the RFB method by augmenting $V_h|_\Sigma$ locally and consider the associated augmented-space formulation.

This can be done by considering, as space of traces Φ_h, the traces of V_h supplemented by a relatively low-dimensional space of traces Φ_e, assuming that any element of Φ_e has support on a single edge. In this way we ensure that the space

$$\Phi_h := V_h|_\Sigma \oplus \Phi_e$$

is defined as the direct sum of its components. Indeed, on any given partition edge γ, the elements of Φ_e are either identically zero, or one-dimensional bubbles, while, by definition, $V_h|_\gamma$ does not contain bubbles. Hence, for any edge γ of the partition, $V_h|_\gamma \cap \Phi_e|_\gamma = \{0\}$.

We consider the associated augmented space V_a, and name the corresponding augmented-space formulation (4) an *enhanced residual-free bubble* (RFBe) method.

Moreover, given the decomposition $V_a = V_l \oplus B_h$ discussed above, we define

$$\widetilde{V}_h := \{v \in V_l : v|_\Sigma \in V_h|_\Sigma\},$$
$$E_h := \{v \in V_l : v|_\Sigma \in \Phi_e\},$$

and call the elements of E_h *edge-bubbles*. Clearly, we have that

$$V_a = \widetilde{V}_h \oplus E_h \oplus B_h. \tag{9}$$

Further, we notice that, by construction, the space of edge-bubbles E_h admits a basis whose elements have their support on the pair of elements sharing a given edge internal to Ω.

The choice of the edge-bubbles or, more precisely, of their traces in Σ, should be dependent on the problem under consideration; indeed, the edge-bubbles may be chosen by exploiting the differential equation or, alternatively, some information about the solution obtained through a previous computation.

In the next section we present an example of a successful application of the RFBe framework and show how an *a priori* error analysis can be used to justify our choice of the edge-bubbles.

3 Increasing the resolution of boundary layers

We exemplify edge-bubbles, designed to capture boundary layer behaviour, and we prove, through *a priori* error analysis, that the particular choice of edge-bubbles results in a reduction of the discretisation error beyond that of the classical RFB method.

Consider the following boundary-value problem for the convection-diffusion equation:

$$\begin{cases} Lu := -\varepsilon \Delta u + \boldsymbol{a} \cdot \nabla u = f & \text{in } \Omega = (0,1)^2, \\ u = 0 & \text{on } \partial\Omega, \end{cases} \tag{10}$$

where the convection field $\boldsymbol{a} \in [\mathrm{C}(\overline{\Omega})]^2$ and the forcing function $f \in \mathrm{L}^2(\Omega)$. In the convection-dominated regime, the solution exhibits a normal (i.e. exponential) boundary layer at the outflow boundary $\partial\Omega_+$; the latter is defined as the set of all points on the boundary $\partial\Omega$ where $\boldsymbol{a} \cdot \boldsymbol{n} > 0$, with $\boldsymbol{n}$ denoting the unit outward normal vector to $\partial\Omega$. Analogously, $\partial\Omega_-$ denotes the inflow boundary, defined as the set of all points on $\partial\Omega$ where $\boldsymbol{a} \cdot \boldsymbol{n} < 0$. It is in the vicinity of the outflow boundary, in particular, that we aim to obtain increased accuracy over a standard Galerkin finite element method and over RFB by a careful choice of edge-bubbles.

3.1 Definition of the RFBe method

Let $\{\mathcal{T}_h\}$ be a family of shape-regular axiparallel partitions of $\overline{\Omega} = (0,1)^2$. Thus, $\mathcal{T}_h$ is the tensor-product of the subdivisions $0 = x_0 < x_1 < \cdots < x_m = 1$ and $0 = y_0 < y_1 < \cdots < y_n = 1$.

We define as *boundary layer region* a neighbourhood of the outflow boundary of width

$$\kappa = \varepsilon \ln(1/\varepsilon), \tag{11}$$

in the direction orthogonal to the boundary (see Figure 1).

We distinguish among those elements that intersect the boundary layer region and those that do not by introducing the subpartitions:

$$\mathcal{T}_{bl} = \{T \in \mathcal{T}_h : \text{dist}(T, \partial\Omega_+) \leq \kappa\}, \tag{12}$$

$$\mathcal{T}_{outer} = \mathcal{T}_h \setminus \mathcal{T}_{bl}. \tag{13}$$

Here, for two subsets A and B of $\mathbb{R}^2$, $\text{dist}(A, B) = \inf_{\mathbf{x}\in A, \mathbf{y}\in B} |\mathbf{x}-\mathbf{y}|$. Accordingly, let Γ_{bl} and Γ_{outer} be the set of all open edges contained in Ω that belong to the elements in $\mathcal{T}_{bl}$ and $\mathcal{T}_{outer}$, respectively. We also define the subset $\Gamma_e \subset \Gamma_{bl}$ containing all open edges with nonempty intersection with the boundary layer region. Furthermore, we denote by Γ_- and Γ_+ the set of all open edges contained in $\partial\Omega_-$ and $\partial\Omega_+$, respectively. Clearly, Γ_e, Γ_{outer}, Γ_- and Γ_+ are mutually disjoint sets and their union is the set of all open element-edges contained in $\overline{\Omega}$. Finally, given any edge γ of an element $T \in \mathcal{T}_h$, we let $h_\gamma := |\gamma|$.

We assume that $h \geq C\kappa$ for some positive constant C and say that the boundary layer is not resolved by the given mesh.

We propose to associate one edge-bubble with each edge $\gamma \in \Gamma_e$ that crosses the boundary layer. Under the above assumption, the number of the edges belonging to Γ_e is $m + n - 2$.

Let T_i, $i = 1, 2$, be the two elements sharing a given edge $\gamma \in \Gamma_e$. We define the edge-bubble e_γ as follows:

- $e_\gamma \in \text{H}_0^1(\Omega)$ and $\text{supp}(e_\gamma) \subset \overline{T_1} \cup \overline{T_2}$;
- the value of e_γ on γ is given by the solution of the one-dimensional boundary-value problem

$$\begin{cases} L_\gamma w = 1 & \text{in } \gamma, \\ w = 0 & \text{on } \partial\gamma, \end{cases} \tag{14}$$

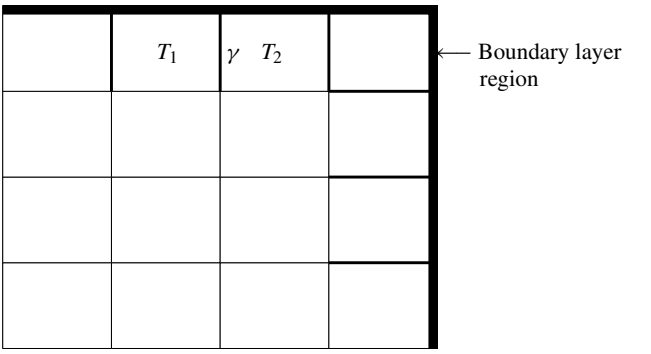

Fig. 1 Axiparallel mesh. Each edge in Γ_e is assigned a single edge-bubble; edges $\gamma \in \Gamma_e$ are indicated in boldface. For example, γ is the shared face of elements T_1 and T_2 and the associated edge-bubble has support $\overline{T_1} \cup \overline{T_2}$

where L_γ is a differential operator obtained from L by considering directional derivatives along γ. In our case, if for example γ is parallel to the y-axis as in Figure 1, then L_γ is obtained on the associated edge $\gamma \in \Gamma_e$ by discarding all terms with derivatives in the x-direction.

– inside T_i, $i = 1, 2$, e_γ satisfies

$$\mathcal{L}_{T_i}(e_\gamma, v) = 0 \qquad \forall v \in \mathrm{H}_0^1(T_i), \tag{15}$$

where $\mathcal{L}_{T_i}$ is the restriction of $\mathcal{L}$ to T_i (as dictated by the definition of E_h).

Remark 2 More generally, when γ is not aligned with a co-ordinate direction, since the Laplacian is rotation-invariant, we would define $L_\gamma w = -\varepsilon w''(t) + a_\gamma w'(t)$, where a_γ is the projection of $\boldsymbol{a}$ along γ.

To handle the case of convection-diffusion equations with symmetric tensor-diffusion coefficient, we would need to freeze the diffusion coefficient to an edge-wise constant tensor. Then a local rotation of the co-ordinate system and stretching along the rotated co-ordinate axis can be used to transform the diffusion term into the Laplacian.

We now introduce the edge-bubble-space

$$E_h := \mathrm{span}\{e_\gamma : \gamma \in \Gamma_e\},$$

and the RFBe method is defined as the Galerkin formulation on the associated augmented space (9).

Alternatively, in order to exploit the well-known approximation properties of the underlying finite element space V_h, we can consider the following equivalent definition. As shown in the previous section, the space of edge-bubbles E_h is in direct sum with B_h and V_h. Thus, as already discussed in the case of the RFB method, we have the following alternative splitting of the augmented space:

$$V_a = V_h \oplus E_h \oplus B_h =: V_P \oplus B_h. \tag{16}$$

Since in (16) we have a direct sum, each $v_a \in V_a$ can be uniquely decomposed as a sum over the three subspaces. Hence, the RFBe formulation reads

$$\begin{cases} \text{find } u_a = u_h + u_e + u_b \in V_a = V_h \oplus E_h \oplus B_h \text{ such that} \\ \mathcal{L}(u_h + u_e + u_b, v_a) = (f, v_a) \qquad \forall v_a \in V_a. \end{cases} \tag{17}$$

Testing in (17) with $v_b \in B_h$, we obtain the bubble equation

$$\mathcal{L}(u_b, v_b) = (f, v_b) - \mathcal{L}(u_h, v_b) \qquad \forall v_b \in B_h, \tag{18}$$

where we have used the orthogonality of E_h and B_h with respect to $\mathcal{L}$ expressed by (15). Starting from the standard RFB formulation (3), we would obtain exactly the same bubble equation. That is to say, the introduction of the edge-bubbles leaves the static condensation procedure unchanged.

Formally, static condensation is carried out as follows. Letting φ_j, $j = 1, \ldots, N_T$, be the local basis functions for V_h on a generic element $T \in \mathcal{T}_h$ and considering the local decomposition $u_{h|_T} = \sum_{j=1}^{N_T} U_j \varphi_j$, we have from (18):

$$u_{b|_T} = \sum_{j=1}^{N_T} U_j b_j + b_f, \tag{19}$$

where

$$\begin{cases} b_j \in \mathrm{H}_0^1(T) \text{ such that} \\ \mathcal{L}(b_j, v) = -\mathcal{L}(\varphi_j, v) \qquad \forall v \in \mathrm{H}_0^1(T), \end{cases} \tag{20}$$

and

$$\begin{cases} b_f \in \mathrm{H}_0^1(T) \text{ such that} \\ \mathcal{L}(b_f, v) = (f, v) \qquad \forall v \in \mathrm{H}_0^1(T). \end{cases} \tag{21}$$

Assume that the variational problems (20) and (21) have been solved. Testing in (17) with $v \in V_P$ and substituting u_b using (19), we arrive at the following problem on the space V_P:

$$\begin{cases} \text{find } u_h + u_e \in V_P \text{ such that} \\ \mathcal{L}(u_h + u_e, v) + \displaystyle\sum_{T \in \mathcal{T}_h} \sum_{j=1}^{N_T} U_j \mathcal{L}_T(b_j, v) = (f, v) - \sum_{T \in \mathcal{T}_h} \mathcal{L}_T(b_f, v) \\ \qquad\qquad\qquad\qquad\qquad\qquad\qquad\qquad\qquad\qquad \forall v \in V_P. \end{cases} \tag{22}$$

Thus, as for the standard RFB method (see, e.g. [6]), the RFBe method results in a generalised Galerkin formulation, this time defined over the locally augmented finite element space $V_P = V_h \oplus E_h$.

We justify the choice of the edge-bubbles through *a priori* analysis.

4 *A priori* error analysis

In the following pages, C represents a constant whose actual value may change at different occurrences; C may depend on $\boldsymbol{a}$, but is always independent of ε and the mesh size h.

We emphasise that the following analysis is valid under the hypothesis that $h \gtrsim \kappa$ (i.e. $h \geq C\kappa$, with $C \geq 1$), where κ is the width of the boundary layer (see (11)). Of course, as the mesh is refined, the relative improvement in accuracy due to the introduction of edge-bubbles gradually diminishes (see the numerical examples below) and, as h becomes smaller, the standard RFB method will yield equally satisfactory results. Indeed, when $h \lesssim \kappa$, even a standard Galerkin finite element method will provide good accuracy. However, our concern here is the case when $h \gtrsim \kappa$.

To proceed, we shall strengthen our hypotheses on the mesh by assuming that it is quasi-uniform, i.e. that there exists a constant $c_0 > 0$ such that

$$c_0 h \leq h_T \leq h = \max_{T \in \mathcal{T}_h} h_T, \tag{23}$$

for every $T \in \mathcal{T}_h$, where h_T is the diameter of the element T.

As regards the data of the problem under consideration (10), we suppose that $\boldsymbol{a} \in [\mathrm{C}^{0,1}(\overline{\Omega})]^2$ and make the further assumption that

$$\boldsymbol{a} = (a_1, a_2)^\top, \qquad \text{where } a_1, a_2 \geq c_a > 0, \tag{24}$$

so that the outflow boundary $\partial\Omega_+$ coincides with the union of the two sides $x = 1$ and $y = 1$. Here, $C^{0,1}(\overline{\Omega})$ denotes the space of Lipschitz-continuous functions defined on $\overline{\Omega}$. For future reference, $C^{1,1/2}(\overline{\Omega})$ will signify the subspace of $C^1(\overline{\Omega})$, the space of continuously differentiable functions on $\overline{\Omega}$, consisting of functions whose first partial derivatives are Hölder-continuous on $\overline{\Omega}$ with exponent $1/2$.

The analysis below is valid as long as internal layers are absent. For this purpose, we assume that f is sufficiently smooth, say, $f \in C^{0,1}(\overline{\Omega})$. Finally, we suppose that $\operatorname{div} \boldsymbol{a} \leq 0$ in Ω to ensure coercivity of the bilinear functional associated with L. Under these hypotheses, the boundary-value problem (10) admits a unique weak solution $u \in H_0^1(\Omega)$.

It follows from the assumptions above that the number of edges belonging to Γ_e (and to Γ_{bl}) is bounded by Kh^{-1} where K is a constant depending only on the quasiuniformity of the mesh. In other words, $\#(\Gamma_e) = \mathcal{O}(1/h)$, while the total number of edges in the partition is of order $\mathcal{O}(1/h^2)$. These facts will be used in the *a priori* analysis.

4.1 Properties of an asymptotic approximation

In order to analyse the RFBe method, we require information about the behaviour of the solution based on performing an asymptotic analysis, — in much the same way as in [21].

We remark that the availability of an asymptotic expansion of the analytical solution u in terms of the small parameter ε is required for analytical purposes but is not needed in the practical implementation of the method.

The reduced problem, corresponding to setting $\varepsilon = 0$ in (10), is defined by

$$\begin{cases} \boldsymbol{a} \cdot \nabla u_0 = f & \text{in } \Omega, \\ u_0|_{x=0} = u_0|_{y=0} = 0, \end{cases} \tag{25}$$

with solution $u_0 \in C^{0,1}(\overline{\Omega})$: in general (i.e. in the absence of additional compatibility conditions on f at the point $(0, 0)$), first-order partial derivatives of u_0 will be discontinuous across the characteristic curve emanating from the inflow corner $(0, 0)$ of $\overline{\Omega}$ (see, e.g., [24], pp. 178).

We consider the asymptotic approximation of u given by

$$\begin{aligned} u_{as}(x, y) = {} & u_0(x, y) - u_0(1, y)\mathrm{e}^{-a_1(1,y)\frac{1-x}{\varepsilon}} - u_0(x, 1)\mathrm{e}^{-a_2(x,1)\frac{1-y}{\varepsilon}} \\ & + u_0(1, 1)\mathrm{e}^{-a_1(1,1)\frac{1-x}{\varepsilon}}\mathrm{e}^{-a_2(1,1)\frac{1-y}{\varepsilon}}, \end{aligned}$$

where the last term is the *corner layer* correction, relevant in the vicinity of $(1, 1)$ where the two boundary layers intersect (see, e.g. [18]). The accuracy of the asymptotic approximation u_{as} depends on the smoothness of the reduced solution u_0. The following result which quantifies the closeness of u_{as} to u has been proved by Schieweck ([27], Lemma 4.4, pp. 33; see also [24], pp. 184).

Lemma 1 *Assume that $a \in [C^1(\overline{\Omega})]^2$, $f \in C^{0,1}(\overline{\Omega})$ and that (24) holds. Given the solution $u \in H_0^1(\Omega)$ of (10) and u_{as} as above, we have that*

$$\varepsilon |u - u_{as}|_{1,\Omega}^2 + ||u - u_{as}||_{0,\Omega}^2 \leq C\varepsilon, \tag{26}$$

where C is a constant independent of ε.

4.2 Characterisation of traces and related results

The *a priori* error analysis is based on the fact that the global error of a locally residual-free finite element method is controlled by the error committed on the skeleton of the partition. For this reason we need to introduce the relevant trace space. The definitions and results from the theory of function spaces summarised here may be found, for instance, in [2] or [29].

The Sobolev space $\mathrm{W}^{k,p}(T)$, $1 \leq p < \infty$, consists of all functions in $\mathrm{L}^p(T)$ whose (weak) partial derivatives of order k and less belong to $\mathrm{L}^p(T)$. When $p = 2$ we shall write $\mathrm{H}^k(T) = \mathrm{W}^{k,2}(T)$. The space $\mathrm{W}^{k,p}(T)$ is equipped with the Sobolev norm $\|\cdot\|_{k,p,T}$ and seminorm $|\cdot|_{k,p,T}$; when $p = 2$, we omit the index p from our notation and simply write $\|\cdot\|_{k,T}$ and $|\cdot|_{k,T}$. For $1 < p < \infty$ the trace of $u \in \mathrm{W}^{1,p}(T)$ on ∂T exists and belongs to the *fractional-order* Sobolev space $\mathrm{W}^{1-1/p,p}(\partial T)$; see, e.g., Adams and Fournier [2].

The fractional-order Sobolev space $\mathrm{W}^{s,p}(\partial T), 0 < s < 1$, can be equipped with an intrinsically defined norm. For instance, when $p = 2$ and $0 < s < 1$, the norm $\|\cdot\|_{s,\partial T}$ and seminorm $|\cdot|_{s,\partial T}$ of the fractional-order space $\mathrm{H}^s(\partial T) = \mathrm{W}^{s,2}(\partial T)$ are defined by

$$\begin{aligned}\|v\|_{s,\partial T} &= \left\{\|v\|_{0,\partial T}^2 + \int_{\partial T}\int_{\partial T} \frac{|v(x) - v(y)|^2}{|x - y|^{1+2s}}\,\mathrm{d}\sigma(x)\,\mathrm{d}\sigma(y)\right\}^{1/2} \\ &= \left\{\|v\|_{0,\partial T}^2 + |v|_{s,\partial T}^2\right\}^{1/2}, \end{aligned} \tag{27}$$

where $d\sigma$ denotes the 1-dimensional Hausdorff measure on ∂T. If γ is a relatively open subset of ∂T, the fractional-order Sobolev space $\mathrm{H}^s(\gamma)$ and its norm $\|\cdot\|_{s,\gamma}$ and seminorm $|\cdot|_{s,\gamma}$ are defined analogously to $\mathrm{H}^s(\partial T)$, $\|\cdot\|_{s,\partial T}$ and $|\cdot|_{s,\partial T}$, respectively.

The Trace Theorem states that the trace on $\partial\hat{T}$ of a function $v \in \mathrm{H}^1(\hat{T})$ belongs to $\mathrm{H}^{1/2}(\partial\hat{T})$ and that there exists a positive constant C such that

$$\|v\|_{1/2,\partial\hat{T}} \leq C\|v\|_{1,\hat{T}} \qquad \forall v \in \mathrm{H}^1(\hat{T}). \tag{28}$$

The properties of the fractional-order space $\mathrm{H}^s(\partial\hat{T})$ as an interpolation space are expressed by the following Interpolation Theorem: given two real numbers $0 \leq s_1 < s_2 \leq 1$ and letting $s = (1 - \theta)s_1 + \theta s_2$, there exists a positive constant C such that

$$\|v\|_{s,\partial\hat{T}} \leq C\|v\|_{s_1,\partial\hat{T}}^{1-\theta}\|v\|_{s_2,\partial\hat{T}}^{\theta} \quad \forall v \in \mathrm{H}^{s_2}(\partial\hat{T}). \tag{29}$$

Let us recall some useful inequalities, which can be proved by scaling arguments applied to the Trace Theorem and the Interpolation Theorem.

Lemma 2 *Let $T \in \mathcal{T}_h$. There exists a constant C, independent of h, such that*

$$|v|_{1/2,\partial T} \leq C|v|_{1,T} \qquad \forall v \in \mathrm{H}^1(T). \tag{30}$$

Furthermore, there exists a constant C, independent of h such that

$$|v|_{1/2,\partial T}^2 \leq C|v|_{1,\partial T}||v||_{0,\partial T} \qquad \forall v \in \mathrm{H}^1(\partial T). \tag{31}$$

In the error analysis we shall also make use of (31) in the form

$$|v|^2_{1/2,\partial T} \leq Ch|v|^2_{1,\partial T} \qquad \forall v \in \mathrm{H}^1(\partial T). \tag{32}$$

This is obtained from (31) by writing $|v|_{1/2,\partial T} = |v - \pi_0(v)|_{1/2,\partial T}$, where $\pi_0(v)$ is the integral mean-value of v over ∂T, and using a standard bound from approximation theory.

Finally we will use the following trace inequality (see, for instance, Brenner and Scott [5]): there exists a positive constant C, independent of h, such that, for any $\alpha > 0$,

$$||v||^2_{0,\partial T} \leq C\left(h^{-1}||v||^2_{0,T} + \alpha^{-1}||v||^2_{0,T} + \alpha|v|^2_{1,T}\right) \quad \forall v \in \mathrm{H}^1(T). \tag{33}$$

4.3 *A priori* error bound

We begin the *a priori* analysis by showing that the global error of a locally residual-free finite element method is governed by the approximation properties of the augmented space V_a on the skeleton of the subdivision.

In order to switch to norms defined over the skeleton of the partition, we shall apply the following result from [25].

Lemma 3 *Assume that $\varepsilon < h \leq 1$, that (23) holds and that the family of partitions $\{\mathcal{T}_h\}$ is shape-regular. Then, for each $T \in \mathcal{T}_h$, each $v_0 \in \mathrm{H}^{1/2}(\partial T)$, and each $w \in \mathrm{H}^1(T)$, there exists a function $v \in \mathrm{H}^1(T)$ with $v = v_0$ on ∂T and satisfying*

$$\varepsilon\,|w - v|^2_{1,T} + \varepsilon^{-1}\,\|w - v\|^2_{0,T} \leq C\left(\varepsilon\,|w - v_0|^2_{1/2,\partial T} + \|w - v_0\|^2_{0,\partial T}\right), \tag{34}$$

where C depends only on the shape-regularity constant of $\{\mathcal{T}_h\}$.

We are now ready to prove the following lemma.

Lemma 4 *Let $u \in V$ and $u_a \in V_a$ be, respectively, the exact solution of (1) and its numerical approximation, the solution of (17). Then the following bound holds:*

$$\varepsilon|u - u_a|^2_{1,\Omega} \leq C \inf_{v_0 \in \Phi_h} \sum_{T \in \mathcal{T}_h} \left(\varepsilon\,|u - v_0|^2_{1/2,\partial T} + \|u - v_0\|^2_{0,\partial T}\right). \tag{35}$$

Proof For any $v \in V_a$, using the appropriate coercivity inequality and Galerkin orthogonality, we have

$$\begin{aligned}
\varepsilon|u - u_a|^2_{1,\Omega} &\leq \mathcal{L}(u - u_a, u - u_a) = \mathcal{L}(u - u_a, u - v) \\
&= \varepsilon\,(\nabla(u - u_a), \nabla(u - v))_\Omega + (\boldsymbol{a} \cdot \nabla(u - u_a), u - v)_\Omega \\
&\leq C\varepsilon|u - u_a|_{1,\Omega}\left(|u - v|_{1,\Omega} + \varepsilon^{-1}||u - v||_{0,\Omega}\right).
\end{aligned}$$

Thus, for any $v \in V_a$,

$$\varepsilon|u - u_a|^2_{1,\Omega} \leq C\left(\varepsilon|u - v|^2_{1,\Omega} + \varepsilon^{-1}||u - v||^2_{0,\Omega}\right). \tag{36}$$

Fix v_0 in Φ_h, the space of traces of V_P over the skeleton of the partition $\mathcal{T}_h$. Applying (34) with $w = u$ we have that, for some $v \in \mathrm{H}_0^1(\Omega)$ which is equal to v_0 on the skeleton of $\mathcal{T}_h$,

$$\varepsilon \, |u - v|_{1,T}^2 + \varepsilon^{-1} \, \|u - v\|_{0,T}^2 \leq C \left(\varepsilon \, |u - v_0|_{1/2,\partial T}^2 + \|u - v_0\|_{0,\partial T}^2 \right),$$

for every $T \in \mathcal{T}_h$. Recalling (36), since $v \in V_a$ and v_0 has been chosen arbitrarily in Φ_h, we conclude the validity of (35). □

Lemma 4 justifies the suggestion that the global error can be reduced by enriching the trial space over the skeleton of $\mathcal{T}_h$ and represents the starting point for the *a priori* error analysis of RFBe.

Theorem 2 *Let $u \in \mathrm{H}_0^1(\Omega)$ be the solution of the boundary-value problem (10), assuming that $\varepsilon > 0$, $f \in \mathrm{C}^{1,1/2}(\overline{\Omega})$ and $\boldsymbol{a} = (a_1, a_2)^\top \in [\mathrm{C}^{1,1/2}(\overline{\Omega})]^2$, with $\operatorname{div} \boldsymbol{a} \leq 0$ and $a_1, a_2 \geq c_a > 0$. Moreover, let $\mathcal{T}_h$ be an axiparallel mesh satisfying (23). Then, as long as $h \geq (1/c_0 c_a)\, \kappa$ and $\varepsilon \leq 1/\mathrm{e}$, the RFB solution $u_{RFB} \in V_{RFB} = V_h \oplus B_h$ (cf. (3)) satisfies*

$$\begin{aligned} &\varepsilon^{1/2} |u - u_{RFB}|_{1,\Omega} + h^{-1/2} ||\boldsymbol{a} \cdot \nabla (u - u_{RFB})||_{-1,\Omega} \\ &\quad \leq C_1 \max \left((\varepsilon / h)^{1/2}, \varepsilon^{1/4} \right) + C_2. \end{aligned} \tag{37}$$

Let $u_a \in V_a = V_h \oplus E_h \oplus B_h$ be the RFBe solution (cf. (17)) where the edge-bubbles are defined according to (15) and (45). Then, under the same hypotheses as above,

$$\begin{aligned} &\varepsilon^{1/2} |u - u_a|_{1,\Omega} + h^{-1/2} ||\boldsymbol{a} \cdot \nabla (u - u_a)||_{-1,\Omega} \\ &\quad \leq C_1 \max \left((\varepsilon / h)^{1/2}, \varepsilon^{1/4} \right) + C_3 h. \end{aligned} \tag{38}$$

The constants C_1, C_2 and C_3 are independent of the mesh size h and of ε, but may depend on $\boldsymbol{a}$.

Proof Applying (35) with $v_0 = u_{as}^I$, an approximation of $u_{as}|_\Sigma$ from Φ_h which will be specified later, we have

$$\begin{aligned} \varepsilon ||u - u_a||_{1,\Omega}^2 &\leq C \sum_{T \in \mathcal{T}_h} \left(\varepsilon |u - u_{as}^I|_{1/2,\partial T}^2 + ||u - u_{as}^I||_{0,\partial T}^2 \right) \\ &\leq C \left(\sum_{T \in \mathcal{T}_h} \left(\varepsilon |u - u_{as}|_{1/2,\partial T}^2 + ||u - u_{as}||_{0,\partial T}^2 \right) \right. \\ &\quad \left. + \sum_{T \in \mathcal{T}_h} \left(\varepsilon |u_{as} - u_{as}^I|_{1/2,\partial T}^2 + ||u_{as} - u_{as}^I||_{0,\partial T}^2 \right) \right) \\ &= C(I + II). \end{aligned}$$

From our assumptions on ε and h it follows that $h \geq c\varepsilon$ with $c = 1/2c_0 c_a$. Thus, using the trace inequalities (30) and (33) with $\alpha = \min\left(\varepsilon^{1/2}, h\right)$, and the bound (26) for the asymptotic approximation u_{as}, we get

$$
\begin{aligned}
I &\leq C \sum_{T\in\mathcal{T}_h} \left((h^{-1}+\alpha^{-1})||u-u_{as}||^2_{0,T} + (\varepsilon+\alpha)|u-u_{as}|^2_{1,T}\right)\\
&\leq C\left((h^{-1}+\alpha^{-1})||u-u_{as}||^2_{0,\Omega} + (\varepsilon+\alpha)|u-u_{as}|^2_{1,\Omega}\right)\\
&\leq C\left(\varepsilon h^{-1} + \varepsilon\alpha^{-1} + \alpha\right)\\
&\leq C\left(\varepsilon h^{-1} + \min\left(\varepsilon^{1/2}, h\right)\right)\\
&\leq C\max\left(\varepsilon h^{-1}, \varepsilon^{1/2}\right).
\end{aligned}
$$

Concerning II, we separate the contributions from those elements that cross the boundary layer region (in which the edge-bubbles are defined), and those that do not:

$$
\begin{aligned}
II \leq & \sum_{T\in\mathcal{T}_{outer}} \left(\varepsilon|u_{as}-u^I_{as}|^2_{1/2,\partial T} + ||u_{as}-u^I_{as}||^2_{0,\partial T}\right)\\
&+ \sum_{T\in\mathcal{T}_{bl}} \left(\varepsilon|u_{as}-u^I_{as}|^2_{1/2,\partial T} + ||u_{as}-u^I_{as}||^2_{0,\partial T}\right)\\
&= III + IV.
\end{aligned}
$$

Let us begin by bounding term III. Consider the decomposition

$$u_{as} = u_0 + u_c,$$

where u_c represents the sum of the three correction terms to u_0 in (26). In the outside-region, since $V_P = V_h$ and u_c is exponentially small there, it is natural to choose, on each edge γ, u^I_{as} as the linear Lagrange interpolant of $u_0|_\gamma$. Hence we set

$$u^I_{as}|_\gamma = \pi_1(u_0|_\gamma) \qquad \forall\gamma\in\Gamma_{outer}\cup\Gamma_-.$$

Note, in particular, that $u_0|_\gamma = 0$ and $u^I_{as}|_\gamma = \pi_1(u_0|_\gamma) = 0$ for all $\gamma\in\Gamma_-$. In addition, we observe that, as $f\in \mathrm{C}^{0,1}(\overline{\Omega})$, we have $u_0\in\mathrm{C}^{0,1}(\overline{\Omega})$, and therefore $u_0\in\mathrm{C}^{0,1}(\bar\gamma)$ for every edge γ; moreover,

$$|u_0|^2_{1,\gamma} \leq Ch_\gamma |u_0'|_{\mathrm{L}^\infty(\gamma)} \leq Ch_\gamma, \tag{39}$$

where u_0' is the derivative of u_0 along the edge γ.

Further, as $u_0\in\mathrm{C}^{0,1}(\overline{\Omega})$, by the definition of u_{as} also $u_{as}\in\mathrm{C}^{0,1}(\overline{\Omega})$. Consequently, the functions u_0, u_{as}, u_c, u^I_{as} appearing below all belong to $\mathrm{H}^1(\partial T)$ for every $T\in\mathcal{T}_h$.

Let $\hat\Gamma_-$ denote the set of all edges in Γ_- that belong to the boundary of some element $T\in\mathcal{T}_{outer}$. Using the triangle inequality, (32), (31) and (39) and a classical interpolation-error bound for the linear Lagrange interpolant (see, e.g., Ciarlet [17]) we have

$$
\begin{aligned}
&\varepsilon \sum_{T\in\mathcal{T}_{outer}} |u_{as}-u^I_{as}|^2_{1/2,\partial T}\\
&\quad\leq 2\varepsilon \sum_{T\in\mathcal{T}_{outer}} \left(|u_0-u^I_{as}|^2_{1/2,\partial T} + |u_c|^2_{1/2,\partial T}\right)
\end{aligned}
$$

$$
\begin{aligned}
&\leq C\varepsilon \sum_{T\in\mathcal{T}_{outer}} \left(h|u_0 - u_{as}^I|_{1,\partial T}^2 + \varepsilon |u_c|_{1,\partial T}^2 + \varepsilon^{-1}\|u_c\|_{0,\partial T}^2 \right) \\
&= C\varepsilon \sum_{\gamma\in\Gamma_{outer}\cup\hat{\Gamma}_-} 2\left(h|u_0 - \pi_1(u_0)|_{1,\gamma}^2 + \varepsilon |u_c|_{1,\gamma}^2 + \varepsilon^{-1}\|u_c\|_{0,\gamma}^2 \right) \\
&\leq C\varepsilon \left(\sum_{\gamma\in\Gamma_{outer}} h|u_0|_{1,\gamma}^2 + \varepsilon \sum_{\gamma\in\Gamma_{outer}\cup\hat{\Gamma}_-} |u_c|_{1,\gamma}^2 + \varepsilon^{-1} \sum_{\gamma\in\Gamma_{outer}\cup\hat{\Gamma}_-} ||u_c||_{0,\gamma}^2 \right) \\
&\leq C\left(\varepsilon + \mathrm{e}^{-2c_0c_a h/\varepsilon} \right) \leq C\varepsilon,
\end{aligned}
$$

due to the estimates of the norms of u_c over the skeleton of the mesh given in the Appendix, and assuming, to obtain the last bound, that $h \geq (1/2c_0c_a)\,\varepsilon \ln(1/\varepsilon)$, which is a slightly less restrictive assumption than what is required by the statement of the theorem.

For the L^2-norm term in III, proceeding in the same fashion, we obtain

$$
\begin{aligned}
\sum_{T\in\mathcal{T}_{outer}} ||u_{as} - u_{as}^I||_{0,\partial T}^2 &\leq 2 \sum_{\gamma\in\Gamma_{outer}\cup\hat{\Gamma}_-} ||u_{as} - u_{as}^I||_{0,\gamma}^2 \\
&\leq 4 \sum_{\gamma\in\Gamma_{outer}\cup\hat{\Gamma}_-} \left(||u_0 - \pi_1(u_0)||_{0,\gamma}^2 + ||u_c||_{0,\gamma}^2 \right) \\
&\leq C\left(\left(\sum_{\gamma\in\Gamma_{outer}\cup\hat{\Gamma}_-} h_\gamma^2 |u_0|_{1,\gamma}^2 \right) + \mathrm{e}^{-2c_0c_a h/\varepsilon} \right) \\
&\leq C\left(\left(\sum_{\gamma\in\Gamma_{outer}\cup\hat{\Gamma}_-} h_\gamma^3 \right) + \mathrm{e}^{-2c_0c_a h/\varepsilon} \right) \\
&\leq C\left(h + \mathrm{e}^{-2c_0c_a h/\varepsilon} \right) \leq Ch.
\end{aligned}
$$

After comparing the two bounds we conclude that

$$
III \leq C(h+\varepsilon) \quad (\leq Ch)\,. \tag{40}
$$

In order to prove this bound on term III we only required that $f \in \mathrm{C}^{0,1}(\overline{\Omega})$ and $\mathbf{a} \in [\mathrm{C}^1(\overline{\Omega})]^2$. We can obtain a sharper bound on III by carefully distinguishing between edges where u_0 has different regularity properties. Suppose, for this end, that $f \in \mathrm{C}^{1,1/2}(\overline{\Omega})$ and $\mathbf{a} \in [\mathrm{C}^{1,1/2}(\overline{\Omega})]^2$. Let Γ_{ns} be the set of all open edges in $\Gamma_{outer} \cup \hat{\Gamma}_-$ that are crossed by the characteristic curve emanating from the point $(0,0)$ and let $\Gamma_{sm} = (\Gamma_{outer} \cup \hat{\Gamma}_-) \setminus \Gamma_{ns}$ be the set of all remaining edges in $\Gamma_{outer} \cup \hat{\Gamma}_-$. Clearly, $\#(\Gamma_{ns}) = \mathcal{O}(1/h)$ due to our hypothesis that $a_1, a_2 > 0$, while $\#(\Gamma_{sm}) = \mathcal{O}(1/h^2)$. Also, $u_0|_\gamma \in \mathrm{C}^{0,1}(\overline{\gamma}) \subset \mathrm{H}^1(\gamma)$ for all $\gamma \in \Gamma_{ns}$, and $u_0|_\gamma \in \mathrm{C}^{1,1/2}(\overline{\gamma})$ for all $\gamma \in \Gamma_{sm}$. Hence,

$$
\begin{aligned}
&\varepsilon \sum_{\gamma\in\Gamma_{outer}\cup\hat{\Gamma}_-} \left(h|u_0-\pi_1(u_0)|^2_{1,\gamma} + h^{-1}\|u_0-\pi_1(u_0)\|^2_{0,\gamma}\right)\\
&\quad = \varepsilon\left(\sum_{\gamma\in\Gamma_{sm}} \left(h|u_0-\pi_1(u_0)|^2_{1,\gamma} + h^{-1}\|u_0-\pi_1(u_0)\|^2_{0,\gamma}\right)\right.\\
&\qquad \left. + \sum_{\gamma\in\Gamma_{ns}} \left(h|u_0-\pi_1(u_0)|^2_{1,\gamma} + h^{-1}\|u_0-\pi_1(u_0)\|^2_{0,\gamma}\right)\right)\\
&\quad \le C\varepsilon\left(\sum_{\gamma\in\Gamma_{sm}} h^3|u_0|^2_{\mathrm{C}^{1,1/2}(\overline{\gamma})} + \sum_{\gamma\in\Gamma_{ns}} h^2|u_0|^2_{\mathrm{C}^{0,1}(\overline{\gamma})}\right)\\
&\quad \le C\varepsilon\left(\sum_{\gamma\in\Gamma_{sm}} h^3 + \sum_{\gamma\in\Gamma_{ns}} h^2\right)\\
&\quad \le C\varepsilon h.
\end{aligned}
$$

Similarly, we gain a factor of h in the analogous bound in the L^2-norm, and we conclude that

$$III \le C(h^2+\varepsilon),$$

where the $\mathcal{O}(\varepsilon)$ term in the bound arises from norms of u_c, in exactly the same way as in (40), our earlier, cruder bound on term III.

We now come to the analysis of IV, i.e. the term concerning norms of $u_{as}-u^I_{as}$ over those elements that intersect the boundary layer. Here we need to distinguish between the edges that belong to Γ_e and those that do not.

We begin by analysing the case $V_P = V_h$, which corresponds to the RFB method. In this case, the value of u^I_{as} along the boundary of the elements belonging to $\mathcal{T}_{bl}$ has already been fixed. Let us concentrate, for instance, on the boundary layer associated with the boundary $y=1$. For each edge $\gamma_i = x_i\times[1-h_\gamma,\,1]\in\Gamma_e$, $i=1,\dots,m-1$, since we have already fixed $u^I_{as}(x_i,1-h_\gamma)=u_0(x_i,1-h_\gamma)$, we have

$$u^I_{as|\gamma_i} = u^i_0(1-h_\gamma)\frac{1-y}{h_\gamma},$$

having introduced the notation $u^i_0(\cdot)=u_0(x_i,\cdot)$. In particular, we notice that since $u^I_{as}|_{\gamma_i}$ vanishes at $y=1$ but $u_0|_{\gamma_i}$ does not, u^I_{as} is no longer the linear interpolant of u_0 along γ_i. Moreover, for every $i=1,\dots,m-1$ we have:

$$|u^I_{as}|^2_{1,\gamma_i} = |u^i_0(1-h_\gamma)|^2h_\gamma^{-1}; \qquad \|u^I_{as}\|^2_{0,\gamma_i} = \frac{1}{3}|u^i_0(1-h_\gamma)|^2h_\gamma.$$

We also note that, by definition, $u^I_{as}|_\gamma = 0$ for all $\gamma\in\Gamma_-\cup\Gamma_+$.

Defining $u_c = u_{as} - u_0$ as before and applying (32) and (31), we have

$$\begin{aligned}
&\varepsilon \sum_{T\in\mathcal{T}_{bl}} |u_{as} - u_{as}^I|^2_{1/2,\partial T} \\
&\quad \le 2\varepsilon \sum_{T\in\mathcal{T}_{bl}} \left(|u_0 - u_{as}^I|^2_{1/2,\partial T} + |u_c|^2_{1/2,\partial T} \right) \\
&\quad \le C\varepsilon \sum_{T\in\mathcal{T}_{bl}} \left(h|u_0 - u_{as}^I|^2_{1,\partial T} + |u_c|_{1,\partial T}\|u_c\|_{0,\partial T} \right). \qquad (41)
\end{aligned}$$

We now split the boundary ∂T of each element $T \in \mathcal{T}_{bl}$ into edges that belong to the union of the sets $\hat{\Gamma}_e = \Gamma_e \cup (\Gamma_- \setminus \hat{\Gamma}_-)$ and Γ_+ and those that belong to $\Gamma_{bl} \setminus \Gamma_e$. Hence, from (41), and noting that $\#(\hat{\Gamma}_e \cup \Gamma_+) = \mathcal{O}(1/h)$ and $\#(\Gamma_{bl}) = \mathcal{O}(1/h)$, we thus obtain:

$$\begin{aligned}
&\varepsilon \sum_{T\in\mathcal{T}_{bl}} |u_{as} - u_{as}^I|^2_{1/2,\partial T} \\
&\quad \le C\varepsilon \sum_{\gamma\in\hat{\Gamma}_e\cup\Gamma_+} \left(h\left(|u_0|^2_{1,\gamma} + |u_{as}^I|^2_{1,\gamma} \right) + \varepsilon|u_c|^2_{1,\gamma} + \varepsilon^{-1}\|u_c\|^2_{0,\gamma} \right) \\
&\qquad + C\varepsilon \sum_{\gamma\in\Gamma_{bl}\setminus\Gamma_e} \left(h|u_0 - u_{as}^I|^2_{1,\gamma} + \varepsilon|u_c|^2_{1,\gamma} + \varepsilon^{-1}\|u_c\|^2_{0,\gamma} \right) \\
&\quad \le C \left(\varepsilon h^{-1} + \varepsilon^2 \sum_{\gamma\in\hat{\Gamma}_e\cup\Gamma_+} |u_c|^2_{1,\gamma} + \sum_{\gamma\in\hat{\Gamma}_e\cup\Gamma_+} ||u_c||^2_{0,\gamma} \right) \\
&\qquad + C\varepsilon \sum_{\gamma\in\Gamma_{bl}\setminus\Gamma_e} \left(h|u_0|^2_{1,\gamma} + h\mathrm{e}^{-2c_0c_a h/\varepsilon} \right) \\
&\quad \le C,
\end{aligned}$$

thanks again to the bounds given in the Appendix.

Similarly, since $(u_{as} - u_{as}^I)|_\gamma = 0 - 0 = 0$ if $\gamma \in \Gamma_+$, for the L^2-norm term in IV we obtain

$$\begin{aligned}
&\sum_{T\in\mathcal{T}_{bl}} \|u_{as} - u_{as}^I\|^2_{0,\partial T} \\
&\quad \le \sum_{\gamma\in\hat{\Gamma}_e\cup\Gamma_+} ||u_{as} - u_{as}^I||^2_{0,\gamma} + \sum_{\gamma\in\Gamma_{bl}\setminus\Gamma_e} ||u_{as} - u_{as}^I||^2_{0,\gamma} \\
&\quad \le 3 \sum_{\gamma\in\hat{\Gamma}_e} \left(||u_0||^2_{0,\gamma} + ||u_{as}^I||^2_{0,\gamma} + ||u_c||^2_{0,\gamma} \right) \\
&\qquad + 2 \sum_{\gamma\in\Gamma_{bl}\setminus\Gamma_e} \left(||u_0 - u_{as}^I||^2_{0,\gamma} + ||u_c||^2_{0,\gamma} \right) \\
&\quad \le C \sum_{\gamma\in\hat{\Gamma}_e} \left(h_\gamma + ||u_c||^2_{0,\gamma} \right) + C \sum_{\gamma\in\Gamma_{bl}\setminus\Gamma_e} \left(h_\gamma|u_0|^2_{1,\gamma} + ||u_c||^2_{0,\gamma} \right) \\
&\quad \le C\left(1 + \varepsilon h^{-1}\right) \le C.
\end{aligned}$$

Thus, for the RFB method,

$$IV \leq C. \tag{42}$$

By considering the case $V_P = V_h \oplus E_h$, we now show that the edge-bubbles proposed provide the required extra resolution in the boundary layer.

Let $T \in \mathcal{T}_{bl}$ and let γ be an edge of T. If $\gamma \in \Gamma_{bl} \setminus \Gamma_e$, then we write $u_{as} = u_0 + u_c$ and since $u_{as}^I|_\gamma = \pi_1(u_0|_\gamma)$ we have:

$$\begin{aligned} |u_{as} - u_{as}^I|_{1,\gamma}^2 &\leq 2\left(|u_0 - \pi_1(u_0)|_{1,\gamma}^2 + |u_c|_{1,\gamma}^2\right) \\ &\leq C\left(|u_0|_{1,\gamma}^2 + \frac{h}{\varepsilon^2}\mathrm{e}^{-2c_0c_ah/\varepsilon}\right) \\ &\leq Ch, \end{aligned} \tag{43}$$

having used the hypothesis that $h \geq (1/c_0c_a)\varepsilon \ln(1/\varepsilon)$ and, once again, the properties presented in the Appendix.

Similarly, if $\gamma \in \Gamma_{bl} \setminus \Gamma_e$, we have:

$$\begin{aligned} \|u_{as} - u_{as}^I\|_{0,\gamma}^2 &\leq 2\left(\|u_0 - \pi_1(u_0)\|_{0,\gamma}^2 + \|u_c\|_{0,\gamma}^2\right) \\ &\leq C\left(h^2|u_0|_{1,\gamma} + h\mathrm{e}^{-2c_0c_ah/\varepsilon}\right) \\ &\leq C\left(h^3 + \varepsilon^2 h\right) \leq Ch^3. \end{aligned} \tag{44}$$

Now, let $\gamma \in \Gamma_e$; consider, for instance, $\gamma_i = x_i \times [1-h_\gamma, 1]$, $i = 1, \ldots, m-1$. In this case, we still have one degree of freedom (the edge-bubble associated with γ_i) at our disposal. That is,

$$u_{as}^I|_{\gamma_i} = u_0^i(1 - h_\gamma)\frac{1-y}{h_\gamma} + g_i e_{\gamma_i},$$

for some coefficient $g_i \in \mathbb{R}$ which we are free to choose. This time we consider the following decomposition of the asymptotic approximation $u_{as}(x, y)$:

$$\begin{aligned} u_{as}(x_i, y) &= u_0(x_i, y) - u_0(x_i, 1)\mathrm{e}^{-a_2(x_i,1)\frac{1-y}{\varepsilon}} \\ &\quad + \left(-u_0(1, y)\mathrm{e}^{-a_1(1,y)\frac{1-x_i}{\varepsilon}} + u_0(1, 1)\mathrm{e}^{-a_1(1,1)\frac{1-x_i}{\varepsilon}}\mathrm{e}^{-a_2(1,1)\frac{1-y}{\varepsilon}}\right) \\ &= u_0^i(y) + u_{c_y}^i(y) + u_c^i(y), \end{aligned}$$

with the notation $u_{c_y}^i(y) = u_0(x_i, 1)\mathrm{e}^{-a_2(x_i,1)\frac{1-y}{\varepsilon}}$.

We wish to choose $u_{as}^I|_{\gamma_i}$ as a good approximation to $u_0^i + u_{c_y}^i$. To this end, consider the decomposition

$$u_0^i + u_{c_y}^i = \left(u_0 + \pi_1(u_{c_y}^i)\right) + \left(u_{c_y}^i - \pi_1(u_{c_y}^i)\right).$$

We observe that $u_{c_y}^i - \pi_1(u_{c_y}^i)$ conforms with our definition of edge-bubble since it solves the homogeneous boundary-value problem

$$\begin{cases} L_{\gamma_i} w = a_2(x_i, 1) \frac{u^i_{c_y}(1-h_\gamma) - u^i_{c_y}(1)}{h_\gamma} & \text{on } \gamma_i \,, \\ w_{|\partial\gamma_i} = 0, \end{cases}$$

where

$$L_{\gamma_i} w := -\varepsilon w'' + a_2(x_i, 1) w'. \tag{45}$$

Thus, with such a definition of L_{γ_i} and recalling (14), we obtain $g_i e_{\gamma_i} = u^i_{c_y} - \pi_1(u^i_{c_y})$ by setting

$$g_i := a_2(x_i, 1) \frac{u^i_{c_y}(1-h_\gamma) - u^i_{c_y}(1)}{h_\gamma}.$$

In this way, recalling the definition of $u^I_{as}|_{\gamma_i}$,

$$\begin{aligned} u^i_0 + u^i_{c_y} - u^I_{as|_{\gamma_i}} &= \left(u^i_0 + \pi_1(u^i_{c_y})\right) + \left(u^i_{c_y} - \pi_1(u^i_{c_y})\right) \\ &\quad - \left(u^i_0(1-h_\gamma)\frac{1-y}{h_\gamma} + g_i e_{\gamma_i}\right) \\ &= u^i_0 + \pi_1(u^i_{c_y}) - u^i_0(1-h_\gamma)\frac{1-y}{h_\gamma} \\ &= u^i_0 + u^i_{c_y}(1)\frac{y-1+h_\gamma}{h_\gamma} + u^i_{c_y}(1-h_\gamma)\frac{1-y}{h_\gamma} \\ &\quad - u^i_0(1-h_\gamma)\frac{1-y}{h_\gamma} \\ &= u^i_0 - \pi_1(u^i_0) + u^i_{c_y}(1-h_\gamma)\frac{1-y}{h_\gamma}, \end{aligned}$$

since $u^i_{c_y}(1) = -u^i_0(1)$.

Hence, using the triangle inequality, the definitions of u^I_{as} and $u^i_{c_y}$, (39) and the definition of u^i_c, we have:

$$\begin{aligned} |u_{as} - u^I_{as}|^2_{1,\gamma_i} &\le 2\left(|u^i_0 + u^i_{c_y} - u^I_{as}|^2_{1,\gamma_i} + |u^i_c|^2_{1,\gamma_i}\right) \\ &= 2\left(\left|u^i_0 - \pi_1(u^i_0) + u^i_{c_y}(1-h_\gamma)\frac{1-y}{h_\gamma}\right|^2_{1,\gamma_i} + |u^i_c|^2_{1,\gamma_i}\right) \\ &\le 4\left(|u^i_0 - \pi_1(u^i_0)|^2_{1,\gamma_i} + h_\gamma^{-1}|u^i_0(1)|^2 \mathrm{e}^{-2a_2(x_i,1)h_\gamma/\varepsilon} + |u^i_c|^2_{1,\gamma_i}\right) \\ &\le C\left(h_\gamma |u^i_0|^2_{1,\gamma_i} + h_\gamma^{-1}\mathrm{e}^{-2c_0 c_a h/\varepsilon} + |u^i_c|^2_{1,\gamma_i}\right) \\ &\le C\left(h^2 + \varepsilon^2 h^{-1} + \varepsilon^{-2} h \mathrm{e}^{-2c_a \frac{1-x_i}{\varepsilon}}\right) \\ &\le Ch. \end{aligned} \tag{46}$$

Similarly,

$$\|u_{as} - u_{as}^I\|_{0,\gamma_i}^2 \leq C\left(h^3 + \varepsilon^2 h + h\mathrm{e}^{-2c_a\frac{1-x_i}{\varepsilon}}\right) \leq Ch^3. \tag{47}$$

We are now ready to bound IV. Note that if $T \in \mathcal{T}_{bl}$ and if γ is an edge of T such that $\gamma \in \Gamma_+$, then $(u_{as} - u_{as}^I)|_\gamma = 0 - 0 = 0$, while if $\gamma \in \Gamma_-$, then $(u_{as} - u_{as}^I)|_\gamma = u_{as}|_\gamma = (u_{as} - u_0)|_\gamma$ and the bounds given in the Appendix apply. Finally, we note that $\#(\Gamma_- \setminus \hat{\Gamma}_-) = 2$. Therefore, using (32), (43) and (46), we have that

$$\begin{aligned}
\varepsilon \sum_{T\in\mathcal{T}_{bl}} |u_{as} - u_{as}^I|_{1/2,\partial T}^2 &\leq C\varepsilon \sum_{T\in\mathcal{T}_{bl}} h|u_{as} - u_{as}^I|_{1,\partial T}^2 \\
&\leq C\varepsilon h\left(\sum_{\gamma\in\Gamma_{bl}} |u_{as} - u_{as}^I|_{1,\gamma}^2 + \sum_{\gamma\in\Gamma_-\setminus\hat{\Gamma}_-} |u_{as} - u_0|_{1,\gamma}^2\right) \\
&\leq C\varepsilon h\left(\sum_{\gamma\in\Gamma_{bl}} h + \sum_{\gamma\in\Gamma_-\setminus\hat{\Gamma}_-} h\varepsilon^{-2}\mathrm{e}^{-2c_a/\varepsilon}\right) \\
&\leq C\varepsilon h.
\end{aligned}$$

As for the L^2-norm term, using, this time, (44) and (47), we have:

$$\begin{aligned}
&\sum_{T\in\mathcal{T}_{bl}} \|u_{as} - u_{as}^I\|_{0,\partial T}^2 \\
&\leq 2\left(\sum_{\gamma\in\Gamma_{bl}} \|u_{as} - u_{as}^I\|_{0,\gamma}^2 + \sum_{\gamma\in\Gamma_-\setminus\hat{\Gamma}_-} \|u_{as} - u_0\|_{0,\gamma}^2\right) \\
&\leq C\left(\sum_{\gamma\in\Gamma_{bl}} h^3 + \sum_{\gamma\in\Gamma_-\setminus\hat{\Gamma}_-} h\mathrm{e}^{-2c_a/\varepsilon}\right) \\
&\leq Ch^2.
\end{aligned}$$

Thus we have shown that

$$IV \leq Ch^2.$$

On adding the bounds on terms III and IV to the bound on term I, we obtain the desired error bounds for RFB and RFBe in the energy-norm $\varepsilon^{1/2}|\cdot|_{1,\Omega}$.

Finally, noting from [26] that the streamline derivative of the error

$$||\boldsymbol{a}\cdot\nabla(u-u_a)||_{-1,\Omega} := \sup_{v\in\mathrm{H}_0^1(\Omega)} \frac{\int_\Omega \boldsymbol{a}\cdot\nabla(u-u_a)v\,\mathrm{d}\Omega}{|v|_{1,\Omega}}$$

is controlled by the energy-norm error, in the sense that

$$h^{-1/2}||\boldsymbol{a}\cdot\nabla(u-u_a)||_{-1,\Omega} \leq C\varepsilon^{1/2}|u-u_a|_{1,\Omega},$$

we deduce that (37) and (38) hold. □

Remark 3 The error bounds stated in the theorem are valid as long as the number of edges crossed by the characteristic curve through (0, 0) is of order $\mathcal{O}(1/h)$, which is true under the hypothesis that $a_1, a_2 > 0$. In the absence of this assumption and requiring that $f \in \mathrm{C}^{0,1}(\overline{\Omega})$ we obtain, by virtue of (40),

$$\begin{aligned}&\varepsilon^{1/2}|u-u_a|_{1,\Omega} + h^{-1/2}||\boldsymbol{a}\cdot\nabla(u-u_a)||_{-1,\Omega}\\ &\quad\le C_1\left((\varepsilon/h)^{1/2}+h^{1/2}\right) + \begin{cases} C_2, & \text{for RFB}\\ C_3 h, & \text{for RFBe.}\end{cases}\end{aligned}$$

We conclude this section with some comments. The correct choice of the trace of the edge-bubble on the common edge of the two elements that form the support of the edge-bubble is hinted by the error analysis: the value of the edge bubble on that edge is equal to the boundary layer correction term in the asymptotic approximation of the solution appearing in the course of bounding the interpolation error $u_{as} - u_{as}^I$. It is this choice that gives rise to the $\mathcal{O}(h)$ term in the error bound (38).

In the context of convection-diffusion problems, we say that a method is uniformly convergent of order α with respect to some norm $||\cdot||_\varepsilon$ (which may depend on ε), if an error bound of the form

$$||u-u_h||_\varepsilon \le Ch^\alpha,$$

holds as $h \to 0$ for some positive constant α that is independent of ε. In the pre-asymptotic regime, when $h \gtrsim \kappa$, we observe for the RFBe method that $\varepsilon^{1/2}|u - u_a|_{1,\Omega} \le Ch$, with C independent of ε.

It is interesting to note that all methods studied in the literature that achieve uniform convergence on a family of shape-regular partitions are based on the use of *ad hoc* exponential basis functions (see [24], pp. 273-8): in particular, we refer to the conforming methods discussed in [23] and [28] and the nonconforming method considered in [1]. Each of these methods includes the use of exponentially fitted splines as trial and test spaces, constructed as tensor products of solutions of the restriction of the original equation on the edges of the partition. They all achieve uniform rate of convergence with $\alpha = 1/2$ in the energy-norm $\varepsilon^{1/2}|\cdot|_{1,\Omega}$.

The method of Schieweck [28], similarly to our method, considers basis functions constructed using exponentials only on those edges which cross the boundary layer; elsewhere, the method uses a standard bilinear approximation. Schieweck proves that, for his method,

$$\varepsilon^{1/2}|u-u_h|_{1,\Omega} \le C\left((\varepsilon/h)^{1/2}+h^{1/2}\right).$$

This bound should be compared with (38) for our RFBe method which can be seen as a combination of the residual-free bubble method with exponential fitting on edges contained in the boundary layer.

We know from the local *a priori* error analysis of Sangalli [25] that, for $\varepsilon \ll h$, away from the boundary layer region, the RFB method is also $\mathcal{O}(h)$ accurate in the energy-norm. Our error bounds show that an identical result cannot hold in the energy-norm on the whole Ω, unless the approximation properties in the layers are improved. Moreover, we have identified the inferior approximation of the boundary layer behaviour along the edges of the partition as the main source of the inaccuracy of the RFB method. This observation will also be confirmed by our numerical experiments.

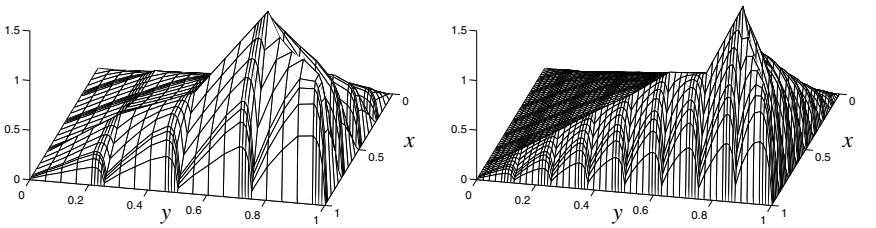

Fig. 2 The RFB solution of the problem from Example 2 on a 4×4 (left) and 8×8 (right) uniform mesh. In both cases the bubbles are computed on an 8×8 Shishkin subgrid. The problem parameters are $\varepsilon = 10^{-2}$, $\boldsymbol{a} = (\cos(\pi/4), \sin(\pi/4))^\top$

Figure 2 may help to clarify why refining the mesh need not improve the accuracy of the RFB method in the preasymptotic regime of $h \gtrsim \kappa$. The plots show the RFB approximation to the solution of the boundary-value problem described in Example 2 below on two subsequent uniform meshes. The lengths of the edges crossing the boundary layer are halved as we half the mesh size, but the number of such edges is doubled. Hence asymptotic convergence is impeded until the mesh starts to resolve the boundary layer.

This argument, of course, can also be seen as further evidence of the advantages of anisotropic mesh refinement. Indeed, returning to the bound (42) on term IV which does not imply convergence of term IV to zero under mesh refinement, we see that this is due to the fact that

$$\sum_{\gamma \in \Gamma_e} h_\gamma = h_\gamma \, \#(\Gamma_e).$$

On a succession of anisotropically refined meshes, graded in the normal direction to the boundary layer, we achieve reduction of h_γ (whilst keeping $\#(\Gamma_e)$ fixed), and hence we should expect improvement in the accuracy of the solution.

5 Full discretisation and numerical examples

As discussed in Section 2, one can consider different splittings of V_{RFB}, the only constraint being that each element of V_{RFB} must be linear on every edge of the partition.

For each $v_h \in V_h$ we define $\widetilde{v}_h \in V_{\text{RFB}}$ such that

$$\begin{cases} \widetilde{v}_h - v_h \in B_h & \text{and} \\ \mathcal{L}(\widetilde{v}_h, v_b) = 0 & \forall v_b \in B_h. \end{cases} \tag{48}$$

In this way we construct a new subspace $\widetilde{V}_h$ which coincides with the space V_l as defined in (5). Moreover, we still have

$$V_{\text{RFB}} = \widetilde{V}_h \oplus B_h,$$

which again leads to the augmented-space formulation discussed in Section 2. Similarly, $V_a = \widetilde{V}_h \oplus E_h \oplus B_h$ where, this time, $\widetilde{V}_h \oplus E_h = V_l$, and the unique solution of (17) can be rewritten as $u_a = \widetilde{u}_h + u_e + u_b^f$ where, as we have seen in Section 2, u_b^f is the solution of

$$\mathcal{L}(u_b^f, v_b) = (f, v_b) \qquad \forall v_b \in B_h.$$

Equivalently, $u_{b\,|_T}^f = b_f$ for any $T \in \mathcal{T}_h$, where b_f solves (21). Further, testing with $w_h \in \widetilde{V}_h \oplus E_h$, we have that $\widetilde{u}_h + u_e$ satisfies

$$\mathcal{L}(\widetilde{u}_h + u_e, w_h) = (f, w_h) - \sum_{T \in \mathcal{T}_h} \mathcal{L}(b_f, w_h) \qquad \forall w_h \in \widetilde{V}_h \oplus E_h, \tag{49}$$

which is equivalent to (8).

The formulation (49) is similar to the *multiscale finite element method* (MFEM) defined in [20] for the solution of symmetric elliptic problems, enhanced by edge-bubbles. The MFEM method is a Galerkin method in which the local basis functions are defined by solving boundary-value problems for the original equation. In our case, given an element $T \in \mathcal{T}_h$ and letting $\{\varphi_i\}_{i=1}^4$ be the standard bilinear basis functions related to T, the corresponding basis functions $\{\widetilde{\varphi}_i\}_{i=1}^4$ for the space $\widetilde{V}_h$ are obtained, according to (48), by solving, for $i = 1, 2, 3, 4$, the local boundary-value problems

$$\begin{cases} \widetilde{\varphi}_i \in \mathrm{H}^1(T) \text{ such that} \\ \mathcal{L}(\widetilde{\varphi}_i, v_b) = 0 \qquad \forall v_b \in \mathrm{H}_0^1(T) \\ \mathrm{Tr}(\widetilde{\varphi}_i) = \varphi_i \qquad \text{on } \partial T. \end{cases} \tag{50}$$

Since the basis functions have to be evaluated numerically, the algorithm is, clearly, of a two-level type.

We have chosen to use the formulation (49)–(50) as the starting point for the full discretisation of the method. Once more, we would like to stress the fact that the two formulations, (22) and (49), are equivalent. Moreover the two approaches involve the same number of subgrid computations. Nevertheless, we have found that the formulation given by (49) is simpler to code and results in slightly faster computations.

In order to solve the boundary-value problems that define the basis functions of V_a, we need to introduce a subgrid. We do so by considering a sub-partition $\mathcal{T}_N$ of the original partition, where N is the discretisation parameter of the new partition. The restriction of $\mathcal{T}_N$ to any element $T \in \mathcal{T}_h$ induces a partition of T that we use to solve the problems (50), (21) and (15) which define, respectively, the local basis for the space $\widetilde{V}_h$, the bubble related to the forcing term and, finally, the edge-bubbles.

Accordingly, on selecting V^N as the bilinear finite element space over $\mathcal{T}_N$, we define:

1. the discrete counterpart of the bubble-space (2) as

$$B^N = B_h \cap V^N;$$

2. the space of edge-bubbles as the subspace of V^N given by

$$E^N = \text{span}\,\{e_j^N,\ j = 1, \ldots, N_e\} \subset V^N,$$

where e_j^N is obtained by solving in V^N the boundary-value problem (15);
3. the discrete counterpart $\widetilde{V}_h^N$ of $\widetilde{V}_h$ as span $\{\widetilde{\varphi}_i^N,\ i = 1, \ldots, 4\}$ for any $T \in \mathcal{T}_h$, where $\widetilde{\varphi}_i^N = \widetilde{\varphi}_i^{N,T}$ is the solution in V^N of (50) on $T \in \mathcal{T}_h$.

The fully discrete RFBe space is then defined as

$$V_a^N = \widetilde{V}_h^N \oplus E^N \oplus B^N,$$

and the fully discrete RFBe formulation reads

$$\begin{cases} \text{find } u_a^N \in V_a^N \text{ such that} \\ \mathcal{L}(u_a^N, v_a^N) = (f, v_a^N) \qquad \forall v_a^N \in V_a^N, \end{cases} \tag{51}$$

and can be again rewritten in the form (49).

The analytical study of the size of the additional error due to the introduction of the subgrid (*subgrid discretisation error*) into the fully discrete formulation (51) does not appear to be straightforward; the main difficulty being that Lemma 3 is no longer applicable at the fully discrete level. Thus, we shall assess the impact of subgrid discretisation on the accuracy of the method through numerical experiments.

5.1 Numerical examples

We now present some numerical experiments in MATLAB©, using the formulation (51) in order to validate the *a priori* error analysis and assess the size of the numerical error due to the discretisation at the subgrid level.

Example 1 We consider the boundary-value problem

$$\begin{cases} Lu := -\varepsilon \Delta u + \boldsymbol{a} \cdot \nabla u = f & \text{in } \Omega, \\ u = g & \text{on } \partial\Omega, \end{cases}$$

where

$$\boldsymbol{a} = \tfrac{1}{2}(3 - xy)(1, 1)^\top; \quad f = 2; \quad g = \begin{cases} (1 + \cos(5\pi x))/2 & \text{if } y = 0 \\ (1 + \cos(3\pi y))/2 & \text{if } x = 0 \\ 0 & \text{otherwise.} \end{cases}$$

We solve this model problem on a sequence of uniform meshes using both the RFB and the RFBe methods. For each computation, the subgrid mesh is axiparallel and of Shishkin type with turning point $\lambda = c_s(\varepsilon/c_a) \ln N$ and the same value of the Shishkin parameter $c_s = 1/4$; see [24] for further details regarding Shishkin meshes.

We wish to confirm the *a priori* bounds on the energy-norm error both in terms of the mesh size h and the diffusion parameter ε. In order to do so, we need to ensure that the subgrid computations are accurate enough.

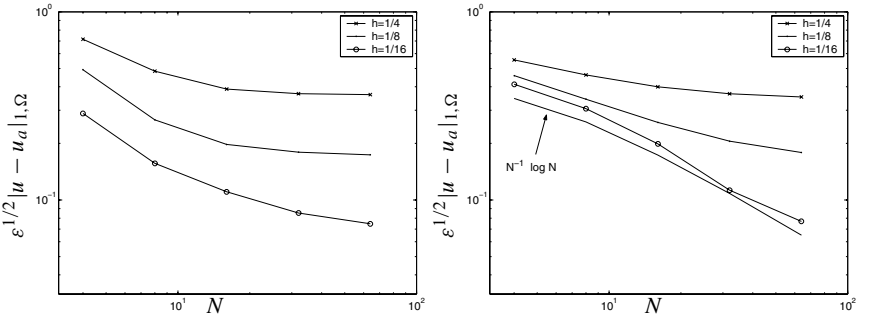

Fig. 3 Example 1. Energy norm error as a function of N: $\varepsilon = 1/50$ (left) and $\varepsilon = 10^{-2}$ (right)

In Figures 3(left) and 3(right) we show the global error in the energy-norm for a fixed mesh size but different values of the subgrid mesh parameter N for, respectively, $\varepsilon = 1/50$ and $\varepsilon = 10^{-2}$.

We notice that a substantial reduction of the error is obtained just by refining the subgrid, until the 'macro-scale' discretisation error becomes dominant and refining the subgrid thereon yields no improvement in the overall accuracy. This happens later for smaller values of ε and h. For instance, for $\varepsilon = 10^{-2}$ and $h = 1/16$ (see Figure 3(right)), we initially observe the characteristic $N^{-1} \log N$ convergence rate on Shishkin meshes (see [24]), showing that the subgrid discretisation error dominates the overall computational error in this case.

Based on such computational evidence, we may infer that the error bound for the fully discrete method should include a term proportional to the error in the numerical approximation of the elemental basis functions. This would be in accordance with the findings of Sangalli [26] on a different augmented RFB formulation applied to a symmetric problem. (For the problems considered in [26], Sangalli's argument is applicable to our method as well).

Convergence in terms of the mesh parameter h is shown in the log-log plots of Figure 4. Since we do not have at hand the exact solution, the error is evaluated using a reference solution given by Richardson extrapolation using two numerical

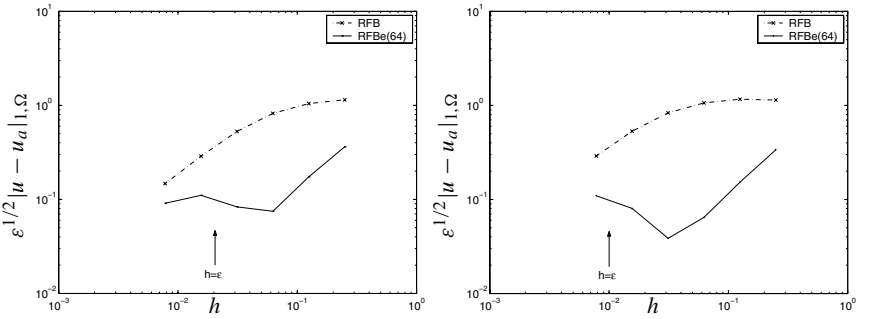

Fig. 4 Example 1. Energy norm error as a function of h for $\varepsilon = 1/50$ (left) and $\varepsilon = 10^{-2}$ (right): RFB method and RFBe method with $N = 64$ (RFBe(64))

Table 1 Example 1. Error and preasymptotic convergence rate for RFBe(64)

	$\varepsilon = 1/50$				$\varepsilon = 10^{-2}$			
h	Energy	rate	L^2	rate	Energy	rate	L^2	rate
1/4	0.36		0.141		0.34		0.17	
1/8	0.17	1.06	0.043	1.7	0.15	1.14	0.051	1.73
1/16	0.07	1.22	0.011	1.92	0.06	1.24	0.0138	1.89
1/32	0.08	−0.15	0.0042	1.43	0.04	0.74	0.0036	1.93
1/64	0.11	−0.41	0.0025	0.77	0.08	−1.05	0.0025	0.53
1/128	0.09	0.28	0.001	1.28	0.11	−0.45	0.0017	0.55

solutions obtained on Shishkin-type meshes with, respectively, 256 and 512 nodes in each co-ordinate direction.

In the preasymptotic regime (i.e. on unresolving meshes of mesh size $h \gtrsim \kappa$) the RFBe solution exhibits first-order 'convergence' to the reference solution in the energy-norm $\varepsilon^{1/2}|\cdot|_{1,\Omega}$; in order to avoid confusion between the decay rate of the error in the preasymptotic regime with the, ultimate, asymptotic convergence rate of the method as $h \to 0$, we shall use the term *preasymptotic convergence rate* to characterise the behaviour of the error for the range of $h \gtrsim \kappa$.

As we keep on refining, the slope of the error curve changes sign (the preasymptotic rate becomes approximately $-1/2$) until the error curve joins the corresponding error curve for the RFB method (the rates are listed in Table 1).

The relatively inaccurate results obtained when $h \sim \varepsilon$ are easy to explain. The region

$$\Omega_{bl} := \left(\cup_{T\in\mathcal{T}_{bl}} \overline{T}\right)^{\circ},$$

where the solution space has been enriched with the edge-bubbles, is properly contained in the boundary layer region, hence part of the boundary layer behaviour cannot be accurately captured. Eventually, the mesh is fine enough to resolve the layer, and the asymptotic convergence rate of the method is then recovered.

As for the subgrid computations, we have used the value $N = 64$ (hence the notation RFBe(64)). We see from Figure 3 that this choice ensures that the subgrid discretisation error is of higher order. For smaller values of ε we can still identify the preasymptotic rate of convergence predicted by our *a priori* analysis; see Figure 5(left).

As regards the L^2-norm error, not covered by our theorem, the preasymptotic convergence rate of the RFBe method appears to be 2. The local *a priori* analysis of Sangalli [25] predicts the same asymptotic rate of convergence for RFB in the outside-region.

So far we have not taken into account computational cost. The RFBe method is computationally more expensive than RFB on the same partition since it involves a larger number of degrees of freedom, and because the extra d.o.f., the edge-bubbles, need to be computed.

Assume, for example, that the partition is uniform with $n \times n$ elements; the number of edge-bubbles is then $2(n-1)$, while the total number of d.o.f. is of $\mathcal{O}(n^2)$. Moreover, assume that the basis functions (50) are calculated using a 4×4 subgrid, as in most of the computations presented so far. As for the edge-bubbles, we are free to consider finer subgrids. We then have a range of possible scenarios.

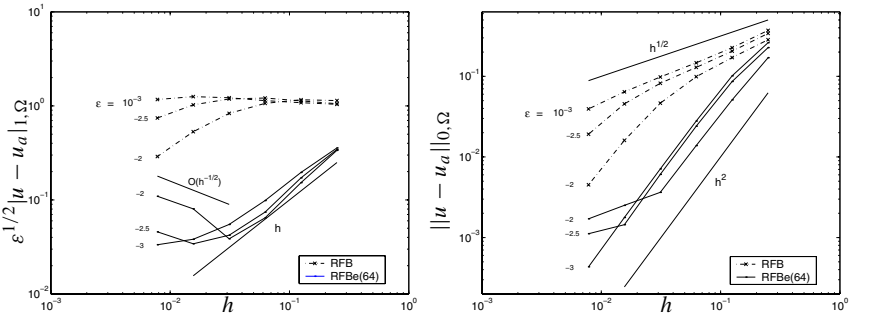

Fig. 5 Example 1. Error as a function of h for different values of ε: the RFB method and the RFBe method with subgrid discretisation parameter $N = 64$ (RFBe(64))

If, for example, the edge-bubbles are also computed on 4×4 subgrids, the computational times for the two methods (RFB and RFBe) are almost identical. On the other hand, if relatively fine subgrids are used for the edge-bubbles (32×32 in our example below), the CPU time is dominated by the computation of the edge-bubbles, hence RFBe then becomes much more expensive than when the coarser 4×4 subgrid is used.

Nevertheless, since the boundary layer is a major source of error, the RFBe method can be more effective even if the edge-bubbles are calculated with high precision. This is particularly true if we require a certain accuracy in the energy-norm of the solution.

In Table 2, we compare the computational time required by a sequential code implementing the RFBe(32), RFBe(4), RFB methods and a standard Galerkin finite element method to compute the solution to a fixed tolerance (TOL) in the energy-norm, for $\varepsilon = 10^{-2}$. (The procedure would be speeded up through parallelisation of the subgrid computations). The table reports the CPU time in seconds on a Pentium III 800 MHz processor; the corresponding number of elements in each co-ordinate direction is given by the numbers in square brackets. We have left the entries of the table blank if in order to achieve the required accuracy a *resolving* mesh was necessary, i.e. if $n > 100$.

Table 2 Example 1. Computational time (in seconds) to achieve, on a uniform mesh, a given accuracy (TOL) in the energy-norm. We indicate in square brackets the number of elements used in each co-ordinate direction on the global uniform mesh. RFBe(N) indicates that an $N \times N$ subgrid was used for computing the edge-bubbles. A 4×4 subgrid is used to compute the RFB (internal) bubbles in each case

	$\varepsilon = 10^{-2}$							
TOL	RFBe(32)		RFBe(4)		RFB		Galerkin	
1/2	6	[3]	2.2	[10]	77	[68]	14	[94]
1/5	16	[7]	59	[58]				
1/10	46	[18]						

Table 3 Example 1. Computational time (in seconds) to achieve, on a uniform mesh, a given accuracy (TOL) in the L^2-norm. We indicate in square brackets, the number of elements used in each co-ordinate direction on the global uniform mesh

	$\varepsilon = 10^{-4}$			
TOL	RFBe(32)	RFBe(4)	RFB	Galerkin
1/5	14 [5]	1 [6]	1.1 [8]	272 [200]
1/10	26 [9]	2.2 [9.8]	14 [30]	
1/50	52 [20]	105 [78]		
1/100	92 [28]			
	$\varepsilon = 10^{-3}$			
TOL	RFBe(32)	RFBe(4)	RFB	Galerkin
1/5	14 [5]	1 [6]	1.8 [10]	5 [62]
1/10	22 [8]	2 [9]	17 [32]	32 [120]
1/50	49 [19]	39 [46]		
1/100	71 [26]	124 [84]		
	$\varepsilon = 10^{-2}$			
TOL	RFBe(32)	RFBe(4)	RFB	Galerkin
1/5	6 [3]	0.6 [4]	1 [6]	0.3 [17]
1/10	14 [6]	1 [6]	2 [16]	0.8 [28]
1/50	35 [14]	4.5 [15]	52 [56]	7 [74]
1/100	52 [20]	9 [22]	137 [90]	21 [106]

We notice that the RFB and Galerkin methods are unable to provide any reasonable accuracy in the energy-norm on unresolving meshes. This situation would become even more evident if we were to consider problems with smaller values of ε. Having said this, the accuracy of the RFBe method on unresolving meshes is also limited albeit to a much lesser extent than the accuracy of RFB and standard Galerkin methods (cf. Figure 5).

Similarly, Table 3 reports the computational time to achieve a fixed accuracy in the L^2-norm, for $\varepsilon = 10^{-2}$, 10^{-3} and 10^{-4}.

Again, the RFBe method is the most effective in almost all the cases considered, in particular for the smaller values of ε. More precisely, we notice the following:

1. For RFBe(32), the evaluation of the edge-bubbles dominates the CPU time;
2. Having said this, the growth of the computational time is roughly linear, while the method converges quadratically (again, see Figure 5);
3. On the other hand, the computational cost of all the other methods considered grows quadratically, while their rate of convergence is less then quadratic.

Hence, as the tolerance becomes tighter, the RFBe(32) method requires a smaller amount of CPU time than the other methods.

Finally, we remark that the mesh used to evaluate the basis functions (the internal bubbles if we think in terms of RFB) could also be adjusted. The presence of the edge-bubbles improves the stability of the RFB method (as we shall show in the next example), hence the same accuracy in the outside-region can be achieved using a poorer approximation to the internal bubbles. For instance, if we switch off the bubbles in the outside-region, we obtain a method similar to the one in [28];

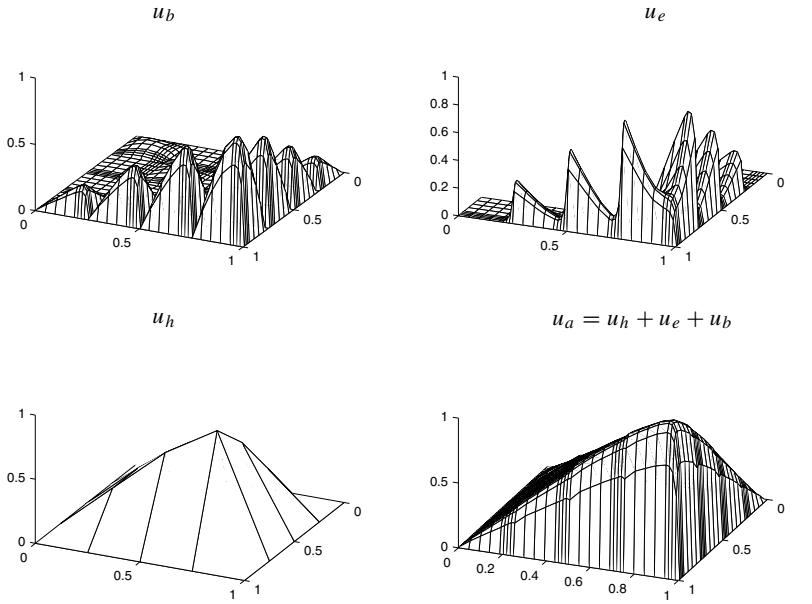

Fig. 6 Example 2. The RFBe solution of the boundary-value problem (52) on a 4×4 uniform mesh for $\varepsilon = 10^{-2}$. The bubbles are computed using a 8×8 Shishkin subgrid

if no other layers are present (as in this example), this yields almost as accurate results as the full RFB method.

Example 2 We solve the boundary-value problem with constant coefficients

$$\begin{cases} -\varepsilon \Delta u + \left(\cos(\frac{\pi}{4}), \sin(\frac{\pi}{4})\right)^\top \cdot \nabla u = 1 & \text{in } \Omega = (0,1)^2, \\ u = 0 & \text{on } \partial\Omega. \end{cases} \tag{52}$$

In Figure 6 we see the numerical solution obtained by using an RFBe method on a uniform mesh with $h = 1/4$ and $\varepsilon = 10^{-2}$ as a sum of its components in the spaces B_h, E_h and V_h.

The convergence in terms of the mesh parameter h in the energy-norm for $\varepsilon = 10^{-2}$ is shown in Figure 7. As for the subgrid computations, we have used axiparallel Shishkin subgrids with $N = 20$ and $N = 4$ and the Shishkin parameter $c_s = 1/2$.

We notice that, for this problem, the error is almost completely concentrated in the boundary layer, so mesh refinement, particularly in the outside-region, is of secondary importance in the regime $h \gtrsim \kappa$.

In contrast with this, as can be seen in Figure 7(right) which reports the error in the outside-region

$$\Omega_{outer} := \Omega \setminus \overline{\Omega_{bl}} = (0, 1-h)^2,$$

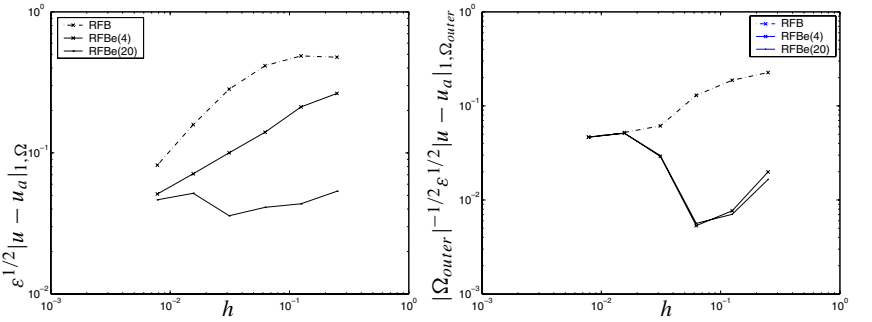

Fig. 7 Example 2. Energy-norm error on Ω (left) and Ω_{outer} (right) as a function of h

the accuracy of the RFBe method away from the boundary layer is largely independent of that of the subgrid computations. As long as $\varepsilon < h$, the numerical solutions obtained by using the RFBe method are more accurate than those delivered by the RFB method: the edge-bubbles have the effect of eliminating the over- and under-shooting near the boundary layer typical of RFB (and of most stabilised finite element methods). This can be seen by comparing Figures 2 and 6.

A similar result was obtained by Mizukami and Hughes [22] with their shock-capturing method which has the additional property of satisfying the discrete maximum principle. Example 4.1 in [22] ($f = 0, \boldsymbol{a} = (\cos(\pi/6), \sin(\pi/6))^\top, \varepsilon = 10^{-7}$ and homogeneous Dirichlet boundary conditions at $x = 1$ and $y = 1$; Dirichlet boundary condition $u = 1$ otherwise) highlights the problem of over- and under-shooting near the boundary layer. The RFBe solution to this problem is nodally very accurate; see Figure 8.

The energy-norm error for different values of ε on a fixed uniform mesh of size $h = 1/8$ is depicted in Figure 9(left). For small values of ε, since we cannot afford to use very fine subgrids, the error due to the approximate computation of the bubbles is dominant. On the other hand, the lower bound on the error given by the error in the outside-region, which is largely independent of the subgrid size, permits us to confirm the *a priori* bounds (see Figure 9(right)).

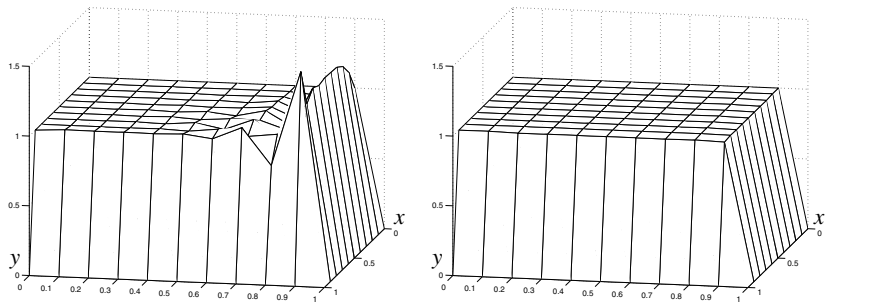

Fig. 8 Solution of Example 4.1 in [22]: $f = 0, \boldsymbol{a} = (\cos(\pi/6), \sin(\pi/6))^\top$, $\varepsilon = 10^{-7}$ and Dirichlet homogeneous boundary conditions at $x = 1$ and $y = 1$; Dirichlet boundary condition 1 otherwise. The edge-bubbles were computed using an 4×4 subgrid. The RFB solution is shown on the left and the RFBe(4) solution on the right

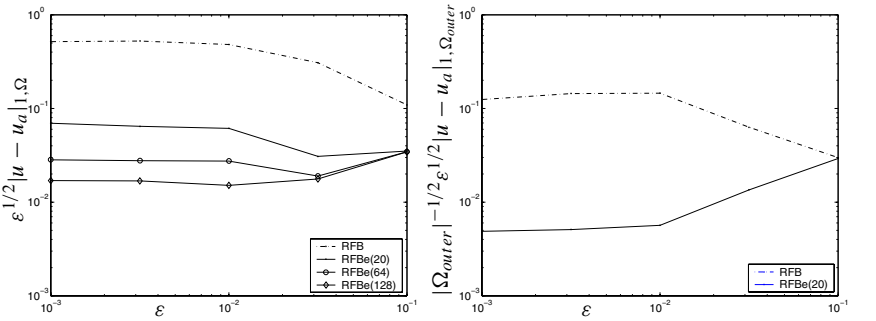

Fig. 9 Example 2. RFB and RFBe energy-norm error on Ω (left) and Ω_{outer} (right) for different values of ε and fixed uniform mesh of size $h = 1/8$

We have verified that the overall accuracy is improved by the introduction of the edge-bubbles. The method achieves both an increased local resolution and a global improvement in accuracy in comparison with RFB (see Figure 7).

In practice, the bases for the bubble-spaces must be evaluated numerically by introducing a subgrid. Since the edge-bubbles are not eliminated via static condensation, one may be led to believe that the method should be quite sensitive to the accuracy to which the numerical solution is to be computed. In fact, this seems to be true only inasmuch as accuracy within the layer is concerned, as we can see by comparing the plots of Figure 7(left) and (right).

Remark 4 In general, one may not know *a priori* in which subregions of Ω the edge-bubbles should be included. Thus, we believe that the RFBe method should be thought of as a corrector in an iteration whose predictor is the RFB method, followed by a loop of *a posteriori* error estimation aimed at locating elements where edge-bubbles need to be inserted; work in this direction is in progress (see [16]).

We conclude with an example taken from [10] and with a remark concerning the application of the RFBe method to problems that exhibit internal layers.

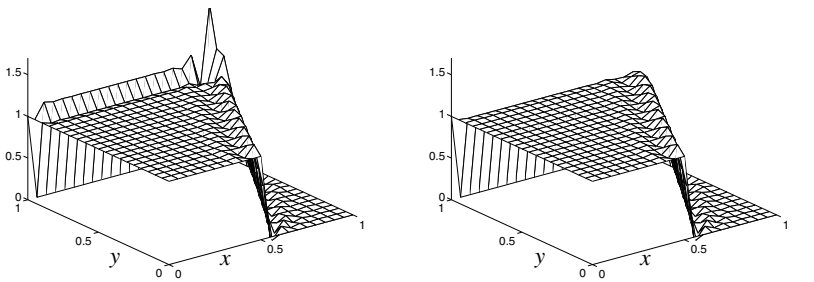

Fig. 10 Example 3. Solution of a problem with an internal layer on a uniform mesh of size $h = 1/20$. The problem parameters are $\varepsilon = 10^{-6}$, $\boldsymbol{a} = (\cos(\pi/3), \sin(\pi/3))^\top$; as for the subgrid, a Shishkin mesh with $N = 4$ has been used. The RFB solution is shown on the left and the RFBe(4) solution on the right

Example 3 We solve the boundary-value problem considered in [10] using the RFB method:

$$\begin{cases} -\varepsilon\Delta u + (\cos(\pi/3), \sin(\pi/3))^\top \cdot \nabla u = 1 & \text{in } \Omega = (0,1)^2, \\ u = 1 \quad \text{for} \begin{cases} x \le 1/2,\ y = 0 \\ x = 0, \end{cases} \\ u = 0 \quad \text{otherwise.} \end{cases} \tag{53}$$

This problem is not covered by our analysis: because of the presence of an internal layer, the asymptotic approximation we used does not satisfy (26). Still, the RFBe results show a considerable improvement over the results delivered by the RFB method.

The solutions obtained by means of the RFB and RFBe methods on a uniform mesh with $h = 1/20$ for $\varepsilon = 10^{-6}$ are shown in Figure 10. We notice that the oscillations near the boundary layer and the spike in the corner layer present in the RFB solution are absent from the RFBe solution. This highlights the fact that such unwanted features of the RFB method are due to poor resolution of the boundary layer on the skeleton of the partition. On the other hand, no visible improvement over the accuracy of RFB is obtained along the internal layer propagating from the point of discontinuity in the boundary condition. One would expect that carefully chosen edge-bubbles defined in a neighbourhood of the internal layer will eliminate this numerical inaccuracy.

6 Conclusions

We have shown how a small number of edge-bubbles can be defined to improve the resolution of boundary layers by the RFB method in the context of convection-dominated-diffusion problems. The resulting RFBe scheme enhances the accuracy of RFB in the preasymptotic regime $h \gtrsim \kappa$. Indeed, both our *a priori* error analysis and our numerical experiments show that on such unresolving meshes the RFB method shows little or no improvement in accuracy in the energy-norm. In contrast, RFBe exhibits the optimal rate of convergence even in the preasymptotic regime.

Moreover, we have noticed that, although we are acting locally, the RFBe scheme delivers increased resolution globally, indicating that the introduction of the edge-bubbles has a stabilising effect. More precisely, our method, similarly to the shock-capturing method presented in [22], shows no over- and under-shooting near the boundary-layer. Such improvement is obtained robustly with respect to the subgrid size and hence at (almost) no extra computational work.

Another characteristic feature of RFBe is that its accuracy inside the boundary layer region is sensitive to the accuracy to which the edge-bubbles have been computed; thus, only if high precision in layers is required, should one consider performing expensive and accurate calculations of the edge-bubbles.

Following the ideas of Brezzi and Marini [14], we presented the RFBe method in a general form, suggesting that other multiscale problems for which the fine scale features are only locally present may benefit from the introduction of edge-bubbles. The principle is that we are ready to afford the introduction of only a small number of new degrees of freedom. In order for the procedure to work efficiently, we must assume that it is known where the bubbles have to be added. This information may

be obtained from previous computations with, or without the use of *a posteriori* error bounds. Of course, instead of selectively adding bubbles, one could also take the opposite approach of selectively removing bubbles. Indeed, we adopted this latter perspective in our recent work [16], in the context of adaptive mesh refinement for convection-dominated diffusion problems: on the coarsest mesh in the sequence of adaptively refined meshes an internal bubble function was included on each element; thereafter, in the process of adaptive mesh refinement, an *a posteriori* error bound was used to selectively turn off the internal bubbles in those elements where they were no longer required from the point of view of achieving a fixed user-prescribed tolerance.

A further direction for future research is the extension of RFBe to problems with internal layers: in the present paper the focus of our work has been the analysis and computational assessment of the method in the case of boundary layers, particularly on unresolving meshes. Numerical experiments indicate that on unresolving meshes one may further reduce the global error by using suitable edge-bubbles within internal layers.

Acknowledgements We are grateful to Professor Franco Brezzi for inspiring this paper. Our work also benefited from discussions with Dr Giancarlo Sangalli which took place at the Isaac Newton Institute in Cambridge, during the program '*Computational Challenges in Partial Differential Equations*' (20 January – 4 July 2003). Andrea Cangiani acknowledges the financial support of INdAM and the EPSRC.

Appendix: Estimates for the asymptotic approximation

As in the main body of the paper, let Γ_{bl} and Γ_{outer} be the set of all open edges contained in Ω that belong to the elements in $\mathcal{T}_{bl}$ and $\mathcal{T}_{outer}$, respectively. We define $\Gamma_e \subset \Gamma_{bl}$ as the set of all open edges in Γ_{bl} with nonempty intersection with the boundary layer region. Furthermore, we denote by Γ_- and Γ_+ the set of all open edges contained in $\partial\Omega_-$ and $\partial\Omega_+$, respectively. Let $\hat{\Gamma}_-$ signify the set of all edges in Γ_- that belong to the boundary of some element $T \in \mathcal{T}_{outer}$.

We shall suppose throughout that $h \geq (1/c_0c_a)\kappa$, where $\kappa = \varepsilon \ln(1/\varepsilon)$ is the thickness of the boundary layer and $\varepsilon \leq 1/\mathrm{e}$.

Lemma 5 *Let $u_c = u_{as} - u_0$ be the collection of all correction terms in the asymptotic approximation u_{as} defined by (26). We have the following bounds.*

a) If $\gamma \in \Gamma_+$, then

$$\varepsilon^2 |u_c|^2_{1,\gamma} + \|u_c\|^2_{0,\gamma} \leq C(h + \varepsilon);$$

b) If $\gamma \in \Gamma_e$, then

$$\varepsilon^2 |u_c|^2_{1,\gamma} + \|u_c\|^2_{0,\gamma} \leq C\varepsilon;$$

c) If $\gamma \in \Gamma_-$, then

$$\varepsilon^2 |u_c|^2_{1,\gamma} + \|u_c\|^2_{0,\gamma} \leq Ch\,\mathrm{e}^{-2c_a/\varepsilon};$$

d) If $\gamma \in \Gamma_{outer} \cup \hat{\Gamma}_-$, then

$$\varepsilon^2 |u_c|^2_{1,\gamma} + \|u_c\|^2_{0,\gamma} \leq Ch\, \mathrm{e}^{-2c_0 c_a h/\varepsilon};$$

e) In addition, the following bound holds:

$$\sum_{\Gamma_{outer} \cup \hat{\Gamma}_-} \varepsilon^2 |u_c|^2_{1,\gamma} + \|u_c\|^2_{0,\gamma} \leq C\, \mathrm{e}^{-2c_0 c_a h/\varepsilon}.$$

Proof The bounds under a) and b) follow from the inequality

$$\begin{aligned}\varepsilon^2 \left(\left| \frac{\partial u_c}{\partial x}(x, y) \right|^2 + \left| \frac{\partial u_c}{\partial y}(x, y) \right|^2 \right) + |u_c(x, y)|^2 \\ \leq C \left(\mathrm{e}^{-2c_a \frac{1-x}{\varepsilon}} + \mathrm{e}^{-2c_a \frac{1-y}{\varepsilon}} + \mathrm{e}^{-2c_a \frac{1-x}{\varepsilon}}\, \mathrm{e}^{-2c_a \frac{1-y}{\varepsilon}} \right),\end{aligned}$$

upon integration over an edge γ belonging to Γ_+ and Γ_e, respectively.

Similarly, the bound c) follows after noting that, for instance,

$$\begin{aligned}\varepsilon^2 \left(\left| \frac{\partial u_c}{\partial x}(0, y) \right|^2 + \left| \frac{\partial u_c}{\partial y}(0, y) \right|^2 \right) + |u_c(0, y)|^2 \\ \leq C \left(\mathrm{e}^{-2c_a/\varepsilon} + \mathrm{e}^{-2c_a/\varepsilon}\, \mathrm{e}^{-2c_a \frac{1-y}{\varepsilon}} \right).\end{aligned}$$

The proof of the bound d) is as follows. Let us suppose that γ is parallel to the x-axis and consider the L^2-norm of the derivative of u_c with respect to x (proceeding in a similar manner, one can prove an analogous bound on the y-derivative of u_c when γ is parallel to the y-axis). It will suffice to consider the first term of u_c, i.e.,

$$u_0(1, y) \mathrm{e}^{-a_1(1,y) \frac{1-x}{\varepsilon}}.$$

We fix an edge $\gamma_{ij} = [x_{i-1}, x_i] \times y_j$ where $i \in \{1, \ldots, m-1\}$ and $j \in \{0, \ldots, m-1\}$. Then,

$$\begin{aligned}&\int_{x_{i-1}}^{x_i} \left| u_0(1, y_j) \frac{\mathrm{d}}{\mathrm{d}x} \mathrm{e}^{-a_1(1,y_j) \frac{1-x}{\varepsilon}} \right|^2 \mathrm{d}x \\ &\quad \leq C \frac{a_1(1, y_j)}{2\varepsilon} \left(\mathrm{e}^{-2a_1(1,y_j) \frac{1-x_i}{\varepsilon}} - \mathrm{e}^{-2a_1(1,y_j) \frac{1-x_{i-1}}{\varepsilon}} \right) \qquad (54) \\ &\quad \leq C\varepsilon^{-2} h\, \mathrm{e}^{-2a_1(1,y_j) \frac{1-x_i}{\varepsilon}} \\ &\quad \leq C\varepsilon^{-2} h\, \mathrm{e}^{-2c_0 c_a h/\varepsilon},\end{aligned}$$

where, in the transition from line two to line three, we applied the Mean Value Theorem to the function $x \mapsto g(x) = \exp(-2a_1(1, y_j) \frac{1-x}{\varepsilon})$ for $x \in [x_{i-1}, x_i]$, and noted that since g' is strictly monotonic increasing on this interval it attains its maximum value at $x = x_i$.

Proceeding in the same manner for the other two terms in u_c, we find that

$$\varepsilon^2 |u_c|^2_{1,\gamma} \leq Ch \mathrm{e}^{-2c_0 c_a h/\varepsilon}.$$

Analogously,

$$\|u_c\|_{0,\gamma}^2 \leq Ch\mathrm{e}^{-2c_0c_ah/\varepsilon},$$

and hence d).

The proof of e) is as follows. Summing (54) over all edges in the set $\Gamma_{outer} \cup \hat{\Gamma}_-$ that are parallel to the x-axis (an identical argument applies to the edges parallel to the y-axis), we get

$$\begin{aligned}
&\sum_{j=0}^{n-1}\sum_{i=1}^{m-1}\int_{x_{i-1}}^{x_i}\left|u_0(1,y_j)\frac{\mathrm{d}}{\mathrm{d}x}\mathrm{e}^{-a_1(1,y_j)\frac{1-x}{\varepsilon}}\right|^2\mathrm{d}x \\
&\quad\leq C\sum_{j=0}^{n-1}\frac{a_1(1,y_j)}{2\varepsilon}\left(\mathrm{e}^{-2a_1(1,y_j)h_\gamma/\varepsilon}-\mathrm{e}^{-2a_1(1,y_j)/\varepsilon}\right) \\
&\quad\leq C\frac{\mathrm{e}^{-2c_ac_0h/\varepsilon}}{\varepsilon h},
\end{aligned}$$

where $h_\gamma = 1 - x_{m-1}$. As $\varepsilon < h$, we deduce that

$$\sum_{j=0}^{n-1}\sum_{i=1}^{m-1}\varepsilon^2\int_{x_{i-1}}^{x_i}\left|u_0(1,y_j)\frac{\mathrm{d}}{\mathrm{d}x}\mathrm{e}^{-a_1(1,y_j)\frac{1-x}{\varepsilon}}\right|^2\mathrm{d}x \leq C\mathrm{e}^{-2c_ac_0h/\varepsilon}.$$

Proceeding in the same manner for the other three terms in u_c, and then repeating the argument for the edges in $\Gamma_{outer} \cup \hat{\Gamma}_-$ that are parallel to the y-axis, we deduce that

$$\sum_{\Gamma_{outer}\cup\hat{\Gamma}_-}\varepsilon^2|u_c|_{1,\gamma}^2 \leq C\,\mathrm{e}^{-2c_0c_ah/\varepsilon}.$$

Analogously,

$$\sum_{\Gamma_{outer}\cup\hat{\Gamma}_-}\|u_c\|_{0,\gamma}^2 \leq C\,\mathrm{e}^{-2c_0c_ah/\varepsilon}.$$

References

1. Adam, D., Felgenhauer, A., Roos, H.-G., Stynes, M.: A nonconforming finite element method for a singularly perturbed boundary value problem. Computing **54**(1), 1–25 (1995)
2. Adams, R.A., Fournier, J.J.F.: Sobolev spaces. Academic Press, New York-London, 2003. Pure and Applied Mathematics, Vol. **140**
3. Bathe, K.-J., Pontaza, J.P.: A flow-condition-based interpolation mixed finite element procedure for higher Reynolds number fluid flows. Math. Models Methods Appl. Sci. **12**(4), 525–539 (2002)
4. Bathe, K.-J., Zhang, H.: A flow-condition-based interpolation finite element procedure for incompressible fluid flows. Comput. & Structures **80**(14–15), 1267–1277 (2002)
5. Brenner, S.C., Scott, L.R.: The mathematical theory of finite element methods. Springer-Verlag, New York, 1994

6. Brezzi, F.: Recent results in the treatment of subgrid scales. In: Canum 2000: Actes du 32e Congrès National d'Analyse Numérique (Port d'Albret), vol. **11** of ESAIM Proc. Soc. Math. Appl. Indust., Paris, 2002, pp 61–84 (electronic)
7. Brezzi, F., Bristeau, M.O., Franca, L.P., Mallet, M., Rogé, G.: A relationship between stabilized finite element methods and the Galerkin method with bubble functions. Comput. Methods Appl. Mech. Engrg. **96**(1), 117–129 (1992)
8. Brezzi, F., Franca, L.P., Hughes, T.J.R., Russo, A. $b = \int g$. Comput. Methods Appl. Mech. Engrg. **145**(3–4), 329–339 (1997)
9. Brezzi, F., Franca, L.P., Hughes, T.J.R., Russo, A.: Stabilization techniques and subgrid scales capturing. In: The State of the Art in Numerical Analysis (York, 1996). Oxford Univ. Press, New York, 1997, pp 391–406
10. Brezzi, F., Franca, L.P., Russo, A. Further considerations on residual-free bubbles for advective-diffusive equations. Comput. Methods Appl. Mech. Engrg. **166**(1–2), 25–33 (1998)
11. Brezzi, F., Hauke, G., Marini, L. D., Sangalli, G.: Link-cutting bubbles for the stabilization of convection-diffusion-reaction problems. Math. Models Methods Appl. Sci. **13**(3), 445–461 (2003)
12. Brezzi, F., Marini, D.: Subgrid phenomena and numerical schemes. In: Mathematical modeling and numerical simulation in continuum mechanics (Yamaguchi, 2000), vol. **19** of Lect. Notes Comput. Sci. Engrg. Springer, Berlin, 2002, pp 73–89
13. Brezzi, F., Marini, D., Süli, E.: Residual-free bubbles for advection-diffusion problems: the general error analysis. Numer. Math. **85**(1), 31–47 (2000)
14. Brezzi, F., Marini, L.D.: Augmented spaces, two-level methods, and stabilizing subgrids. Internat. J. Numer. Methods Fluids **40**(1–2), 31–46 (2002)
15. Brezzi, F., Russo, A.: Choosing bubbles for advection-diffusion problems. Math. Models Methods Appl. Sci. **4**(4), 571–587 (1994)
16. Cangiani, A., Süli, E.: A-posteriori error estimators and RFB. Oxford University Computing Laboratory research report NA-04/23, 2004
17. Ciarlet, P.G.: The finite element method for elliptic problems. North-Holland Publishing Co., Amsterdam, 1978. Studies in Mathematics and its Applications, Vol. **4**
18. Eckhaus, W.: Asymptotic analysis of singular perturbations, vol. **9** of Studies in Mathematics and its Applications. North-Holland Publishing Co., Amsterdam, 1979
19. Franca, L.P., Madureira, A., Valentin, F.: Towards multiscale functions: enriching finite element spaces with local but not bubble-like functions. Comput. Methods Appl. Mech. Engrg. 2003
20. Hou, T.Y., Wu, X.-H.: A multiscale finite element method for elliptic problems in composite materials and porous media. J. Comput. Phys. **134**(1), 169–189 (1997)
21. Hou, T.Y., Wu, X.-H., Cai, Z.: Convergence of a multiscale finite element method for elliptic problems with rapidly oscillating coefficients. Math. Comp. **68**(227), 913–943 (1999)
22. Mizukami, A., Hughes, T.J.R.: A Petrov-Galerkin finite element method for convection-dominated flows: an accurate upwinding technique for satisfying the maximum principle. Comput. Methods Appl. Mech. Engrg. **50**(2), 181–193 (1985)
23. O'Riordan, E., Stynes, M.: A globally uniformly convergent finite element method for a singularly perturbed elliptic problem in two dimensions. Math. Comp. **57**(195), 47–62 (1991)
24. Roos, H.-G., Stynes, M., Tobiska, L.: Numerical Methods for Singularly Perturbed Differential Equations. Springer-Verlag, Berlin, 1996.
25. Sangalli, G.: Global and local error analysis for the residual-free bubbles method applied to advection-dominated problems. SIAM J. Numer. Anal. **38**(5), 1496–1522 (2000) (electronic)
26. Sangalli, G.: Capturing small scales in elliptic problems using a residual-free bubbles finite element method. Multiscale Modeling and Simulation: A SIAM Interdisciplinary Journal **1**(3), 485–503 (2003)
27. Schieweck, F.: Eine asymptotisch angepaßte Finite-Element-Methode für singulär gestörte elliptische Randwertaufgaben. Dissertation, TH Magdeburg, 1986
28. Schieweck, F.: Numerische integration bei der finite-element-diskretisierung singulär gestörten elliptischer randwertaufgaben. Wiss. Z. Techn. Universität Magdeburg, 1987
29. Triebel, H.: Interpolation theory, function spaces, differential operators. VEB Deutscher Verlag der Wissenschaften, Berlin, 1978